

Uncertainty-enabled Thermal Stress Management of Engineered Multilayered Structures

Sameed Ahmed¹, Johannes Brust², Cassie Marker³, Paul Miles⁴, Siamak Rabieniaharatbar⁵ Peter Wills⁶

Problem Presenter: Jordan Massad, Robert Kuether⁷; Faculty Mentors: Ralph Smith⁸

Abstract

Multilayered structures are of importance for a variety of industrial applications. The temperature at which they are made and used can differ greatly, which can effect the structures' reliability due to resulting residual stress and deflection. The trial-and-error method often used by experimentalists has improved multilayered structure design, but this approach lacks efficiency in producing desired results. Mathematical modeling, simulation, and computation of multilayered structures provide a way to streamline the process of choosing design parameters for desired results. In this paper, we take an existing model of thermal deformation of multilayered structures and expand it by including temperature dependence of material properties and layer gradation. We demonstrate the efficacy of the model by applying it to three representative structures. We then further analyze multilayered structures both analytically and numerically by studying the models sensitivity, optimization, and uncertainty. We conclude by summarizing our observations and providing design suggestions.

1 Introduction

Multilayered structures are critical for a large number of applications including microelectronics, thermal barrier coatings, and ceramic capacitors. Depending on the application, the multilayers can be a combination of different classes of materials such as, ceramics, metals, polymers, or solders. Materials are combined due to the necessity of achieving certain service conditions of a part. These service conditions vary with location and therefore the material requirements also vary with location. For example, a multilayered high temperature co-fire ceramic is combined with aluminum to form a microelectronic device package with an integral window as shown in a report by Peterson and Watson [4]. More recently, the use of additive manufacturing has allowed for the creation of gradient materials. Carroll et al. [1] investigated the creation of a pure Inconel 625 to pure Stainless Steel 304L graded sample. Zhang et al. [5] investigated the creation of a gradient thermal barrier coating going from $\text{ZrO}_2\text{Y}_2\text{O}_3$ to NiCrAlY.

An intrinsic difficulty with multilayered structures is that the combination of different materials can cause the formation of residual stresses or deflection. Residual stress is defined as the stress present in the object while in the absence of any external load or force [3], while deflection is the related to the degree of curvature of the material [2]. The introduction of deflection or residual stress is due to the differing mechanical properties and processing parameters of the creation of the materials. When a multilayered material is heated or cooled, the materials in each layer expand and contract differently. If the expansion or contraction is inhibited by the other layers, then residual stress is introduced. If the expansion or contraction of the layers is partially allowed, it causes the material to curve.

A typical method for creating multilayered structures is through trial-and-error. However, the use of modeling, computational tools, and software to predict specific properties can narrow down experimental options, which saves time and money by greatly reducing the need of trial-and-error.

This work presents the formation of a computational tool that allows for the robust design of multilayered structures given certain specifications and outputs the temperature dependent residual stress and deflection. This tool allows for uncertainty quantification and the ability to optimize the residual stress and deflection to specific variables of interest.

¹Applied Math, University of South Carolina

²Applied Math, University of California Merced

³Materials Science and Engineering, Pennsylvania State University

⁴Mechanical Engineering, Florida State University

⁵Math, Purdue University

⁶Applied Math, University of Colorado

⁷Sandia National Laboratory

⁸North Carolina State University

The structure of this report is as follows. Section 2 formally defines the problem and model used. Section 3 outlines the testing of the model, sensitivity analysis, design optimization and uncertainty quantification. Section 4 summarizes our work and provides suggestions for future capability enhancement.

2 The Problem

To be able to develop a computational tool, we first have to build a forward model that calculates the residual stress and deflection. Second, we also need to be able to minimize the residual stress and deflection and optimize different variables while providing uncertainty quantifications.

2.1 The Forward Model

The first step is to define the design parameters of multilayered structures below:

T_{ref}	The temperature where the strain and the stress are zero
T_{\min}	The minimum temperature that the material is subject to
T_{\max}	The maximum temperature the material is subject to
m	The gradient exponent
E_i	Young's modulus of each material i (Temperature dependent)
n	Number of layers in a gradient layer
N	Number of layers
h	Total thickness of the multilayered material
z_i	Thickness of layer i
ν_i	Poisson's ratio of each layer i (Temperature dependent) ($0 < \nu < 0.5$)
$\varepsilon_i^{\text{th}}$	Thermal strain of each layer i (Temperature dependent)

Table 1: The important design variables for multilayered structures.

From these variables we started with Hall's [2] model by defining the stress in Cartesian coordinates as

$$\varepsilon_x = \varepsilon^{\text{th}} + [\sigma_x - \nu(\sigma_y + \sigma_z)]/E \quad (1)$$

$$\varepsilon_y = \varepsilon^{\text{th}} + [\sigma_y - \nu(\sigma_x + \sigma_z)]/E \quad (2)$$

$$\varepsilon_z = \varepsilon^{\text{th}} + [\sigma_z - \nu(\sigma_x + \sigma_y)]/E, \quad (3)$$

where ε_x , ε_y , ε_z are the strains along the x, y, and z directions, and σ_j is the stress. We then assume an axisymmetric disk in the $x - y$ plane, which implies $\sigma_z = 0$ and due to symmetry $\varepsilon_x = \varepsilon_y$ and $\sigma_x = \sigma_y$. This leads to the simplification

$$\varepsilon = \varepsilon^{\text{th}} + \sigma(1 - \nu)/E \quad (4)$$

where we remove subscripts to simplify notation. Recall that z is the coordinate corresponding to the thickness of the plate. Assuming the strain is a linear function of z , the strain can then be written as

$$\varepsilon = \varepsilon_B + \frac{z}{h}(\varepsilon_T - \varepsilon_B), \quad (5)$$

where T and B refer to the top and bottom of the plate, respectively. We consider that for a plate consisting of i layers, each layer will have its own set of material properties. Therefore the stress within the i^{th} layer can be found by combining (4) and (5), yielding the stress at the boundaries:

$$\sigma_i = \frac{E_i}{1 - \nu_i} \left(\varepsilon_B + \frac{z}{h}(\varepsilon_T - \varepsilon_B) - \varepsilon_i^{\text{th}} \right). \quad (6)$$

In our model, we assume quasi-static equilibrium, allowing us to calculate the stress at a given temperature without considering any rate effects. The equilibrium equations are then:

$$\sum_i^N P_i = 0, \sum_i^N M_i = 0 \quad (7)$$

where P_i is the radial force per unit perimeter in the i^{th} layer, and M_i is the moment per unit perimeter. The force and moment are defined with respect to (6) by

$$P_i = \int_{z_{i-1}}^{z_i} \sigma dz = \frac{E_i}{1 - \nu_i} \left((\varepsilon_B - \varepsilon_i^{th})(z_i - z_{i-1}) + \frac{(\varepsilon_T - \varepsilon_B)(z_i^2 - z_{i-1}^2)}{2h} \right) \quad (8)$$

$$M_i = \int_{z_{i-1}}^{z_i} z \sigma dz. \quad (9)$$

After simplification, we find that

$$\varepsilon_{top} = \frac{1}{F} \left[(C_2 - D_2)[6h(A_1 - B_1) - 3(A_2 - B_2)] + (C_1 - D_1)[4(A_3 - B_3) - 6h(A_2 - B_2)] \right] \quad (10)$$

$$\varepsilon_{bottom} = \frac{1}{F} \left[4(A_3 - B_3)(C_1 - D_1) - 3(A_2 - B_2)(C_2 - D_2) \right], \quad (11)$$

where

$$F = 4(A_1 - B_1)(A_3 - B_3) - 3(A_2 - B_2)^2 \quad (12)$$

$$A_k = \sum_i^N \bar{E}_i z_i^k \quad (13)$$

$$B_k = \sum_i^N \bar{E}_i z_{i-1}^k \quad (14)$$

$$C_k = \sum_i^N \bar{E}_i \varepsilon_i^{th} z_i^k \quad (15)$$

$$D_k = \sum_i^N \bar{E}_i \varepsilon_i^{th} z_{i-1}^k. \quad (16)$$

Here $\bar{E}_i = E_i / (1 - \nu_i)$ is the biaxial modulus and z_i is the z -location of the top of the i^{th} layer. From these simplified equations the mag stress in the middle of the layers can be calculated:

$$\sigma_{mag} = \left[\frac{(\sigma_i + \sigma_{i-1})^2 - \sigma_i \sigma_{i-1}}{3} \right]^{\frac{1}{2}} \quad (17)$$

The radius of curvature is found to be

$$\rho = \frac{h}{\varepsilon_T - \varepsilon_B}, \quad (18)$$

where ρ is the radius of curvature and h is the thickness of the total multilayered material. From ρ the deflection can be calculated as

$$\delta = sign(\rho) \left(|\rho| - \sqrt{\rho^2 - R^2} \right), \quad (19)$$

where R is the radius of the axisymmetric disk. This model also assumes that $|\rho| > R$ and that $|\delta| < h$. At this point in the model, the deflection, stress in the middle of a layer and the stress at the boundaries of the layer can be calculated. Hall's model assumes that each layer has uniform properties. However, with a gradient layer that is not the case and thus needs to be addressed.

2.2 Gradient Layers

In order to deal with gradient layers, we implemented the work by Zhang et al.[5]. Assuming layer i starts with pure material R and is graded to pure material S, the layer is divided into sublayers n . Then uniform properties are assumed for each sublayer by finding the E_n , ε_n^{th} , and ν_n by

$$E_n = E_R \left(\frac{z}{t_n} \right)^m + E_S \left(1 - \left(\frac{z}{t_n} \right) \right)^m \quad (20)$$

$$\nu_n = \nu_R \left(\frac{z}{t_n} \right)^m + \nu_S \left(1 - \left(\frac{z}{t_n} \right) \right)^m \quad (21)$$

$$\varepsilon_n = \varepsilon_R \left(\frac{z}{t_n} \right)^m + \varepsilon_S \left(1 - \left(\frac{z}{t_n} \right) \right)^m \quad (22)$$

At this point the temperature dependence of the thickness and material properties must be determined.

2.3 Temperature Dependence

Since the strip is much thinner in the z -direction than in the x - and y -directions, we have assumed that the thermal deformation of each sub-layer thickness is negligible. However, for certain materials and applications, this thickness deformation needs to be accounted for. We determine the effect of thickness deformation on stress, radius of curvature, and deformation analytically and numerically. Thickness deformation is given by

$$z_i = \gamma_i z_{i0}, \quad (23)$$

where z_{i0} is the thickness of layer i before thermal deformation, z_i is the thickness of layer i after thermal deformation, and γ_i is the factor by which the thickness of layer i deforms. We assume uniform thickness deformation, that is, each sub-layer deforms by the same factor. We then find that

$$\gamma_i = \gamma, \quad i = 1, \dots, N. \quad (24)$$

Upon inspection of the formulas for top strain, (11), and bottom strain, (12), it can be seen that the numerators and denominators both have thickness to the fourth power. Since the factor for thickness deformation is the same in each sub-layer, this factor can be factored out each term in the numerator and denominator and canceled. Therefore, top strain and bottom strain are invariant to thickness deformation. The only remaining term in the stress that depends on the thickness deformation is $\frac{z}{h}$. Again, the thickness deformation factor cancels out here. Therefore, the stress is also invariant to thickness deformation. As seen in (19), the radius of curvature linearly depends on thickness deformation,

$$\rho = \gamma \rho_0. \quad (25)$$

For $\rho > 0$ the deflection is given by

$$\delta = \rho - \sqrt{\rho^2 - L^2} \quad (26)$$

$$= \frac{L^2}{\rho + \sqrt{\rho^2 - L^2}} \quad (27)$$

$$\approx \frac{L^2}{2\rho} \quad (28)$$

$$\approx \frac{1}{\gamma} \delta_0, \quad (29)$$

where the second equality is from multiplying by the conjugate and simplifying, and the third approximation is due to $L \ll \rho$. Thus the deflection depends on thickness deformation inversely linearly.

For the numerical test, we used the example in Hall [2]. We vary each sub-layer thickness within 10% ($0.90 \leq \gamma \leq 1.10$). The stress in the middle of each layer, radius of curvature, and deformation are tracked

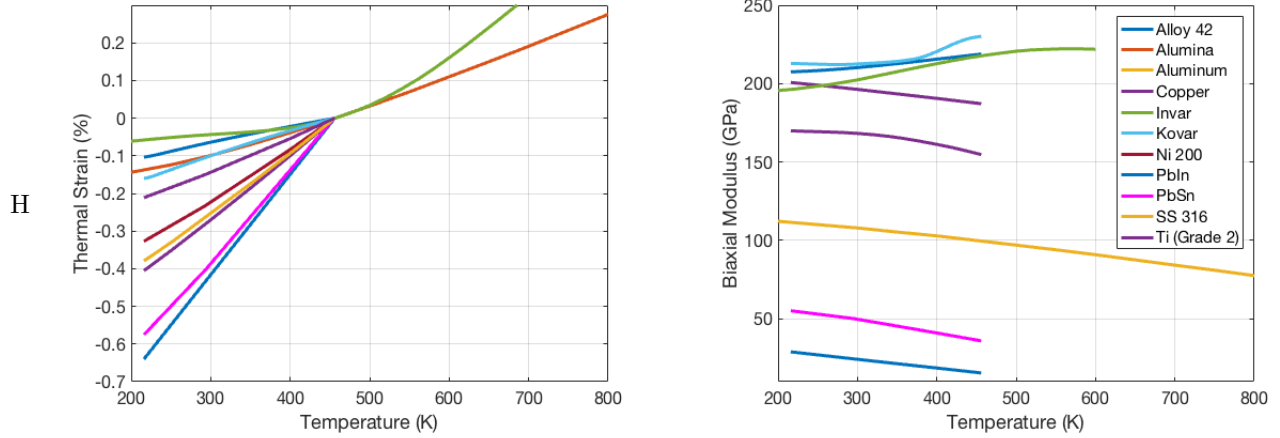


Figure 1: This a graphical showing of the temperature dependence of multiple materials properties.

with varying thickness. The results match our analytical results. So for this work the temperature dependence of the thickness has found to be negligible and not included.

Up to this point the assumption has been made that the materials properties, E_i , ε_i , and ν_i are constant, when in reality these properties vary with temperature as discussed in the table above. An example of the variance of materials properties as a function of temperature is shown below:

To handle the temperature dependence, tables of the variables at discrete temperatures are inputted and a linear interpolation is done to the temperatures of interest for the specific problems. With the forward model in place, testing, sensitivity, optimization and uncertainty were implemented.

3 The Approach

3.1 Forward Model Testing

To test the model three different realistic problems were tested and are presented here.

Problem A) The 5 layered material is shown below. The T_{ref} was set to 456 K, T_{min} was set to 298, and the T_{max} was set 456. The thicknesses of the solder and the gradation variable m were. When $m = 0.25$ it means the gradient layer contains more Titanium and when $m = 2$ it means the gradient layer contains more Invar. The effects of changing m are graphically shown in 2 as well.

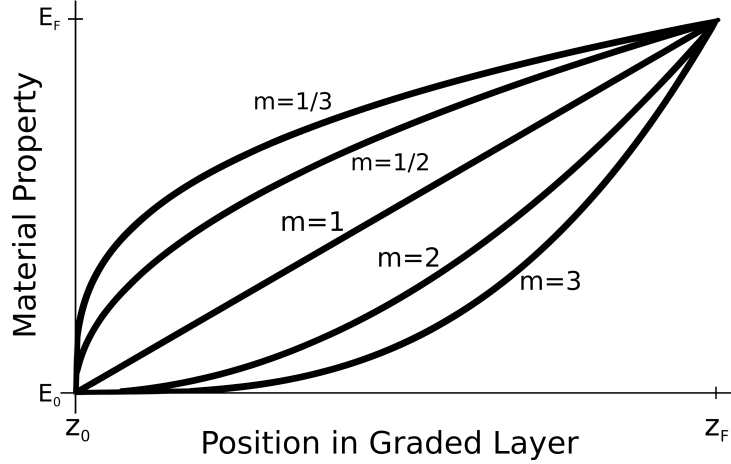


Figure 2: When $m=1$ the change between material E_0 and E_F is linear but when $m > 1$ then there is more E_0 before going to E_F and when $m < 1$ then there is more E_F .

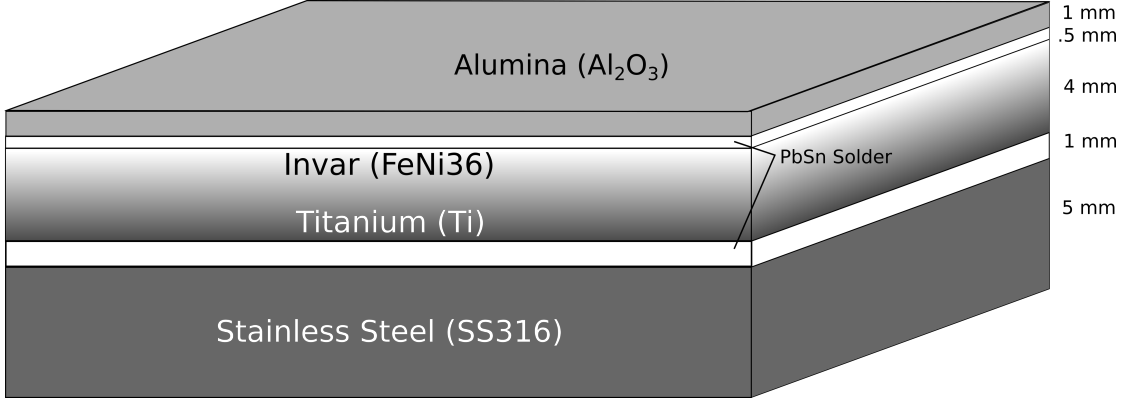


Figure 3: A picture of the set up for problem A.

Case 1	Case 2	Case 3	Case 4
Alumina $z = 1 \text{ mm}$	Alumina $z = 1 \text{ mm}$	Alumina $z = 1 \text{ mm}$	Alumina $z = 1 \text{ mm}$
PbSn solder $z = 0.1 \text{ mm}$	PbSn solder $z = 0.5 \text{ mm}$	PbSn solder $z = 0.1 \text{ mm}$	PbSn solder $z = 0.5 \text{ mm}$
Invar gradation Titanium Grade 2 $z = 4 \text{ mm}$ $n = 50$ $m = 0.5$	Invar gradation Titanium Grade 2 $z = 4 \text{ mm}$ $n = 50$ $m = 0.5$	Invar gradation Titanium Grade 2 $z = 4 \text{ mm}$ $n = 50$ $m = 2$	Invar gradation Titanium Grade 2 $z = 4 \text{ mm}$ $n = 50$ $m = 2$
PbSn solder $z = 0.2 \text{ mm}$	PbSn solder $z = 1.0 \text{ mm}$	PbSn solder $z = 0.2 \text{ mm}$	PbSn solder $z = 1.0 \text{ mm}$
Stainless Steel 316 $z = 5 \text{ mm}$	Stainless Steel 316 $z = 5 \text{ mm}$	Stainless Steel 316 $z = 5 \text{ mm}$	Stainless Steel 316 $z = 5 \text{ mm}$

Table 2: The different cases studied for problem A.

The variation in solder thickness and m were studied. In Figure 4 Case 1 and 2 with $m = 0.5$ is on the left

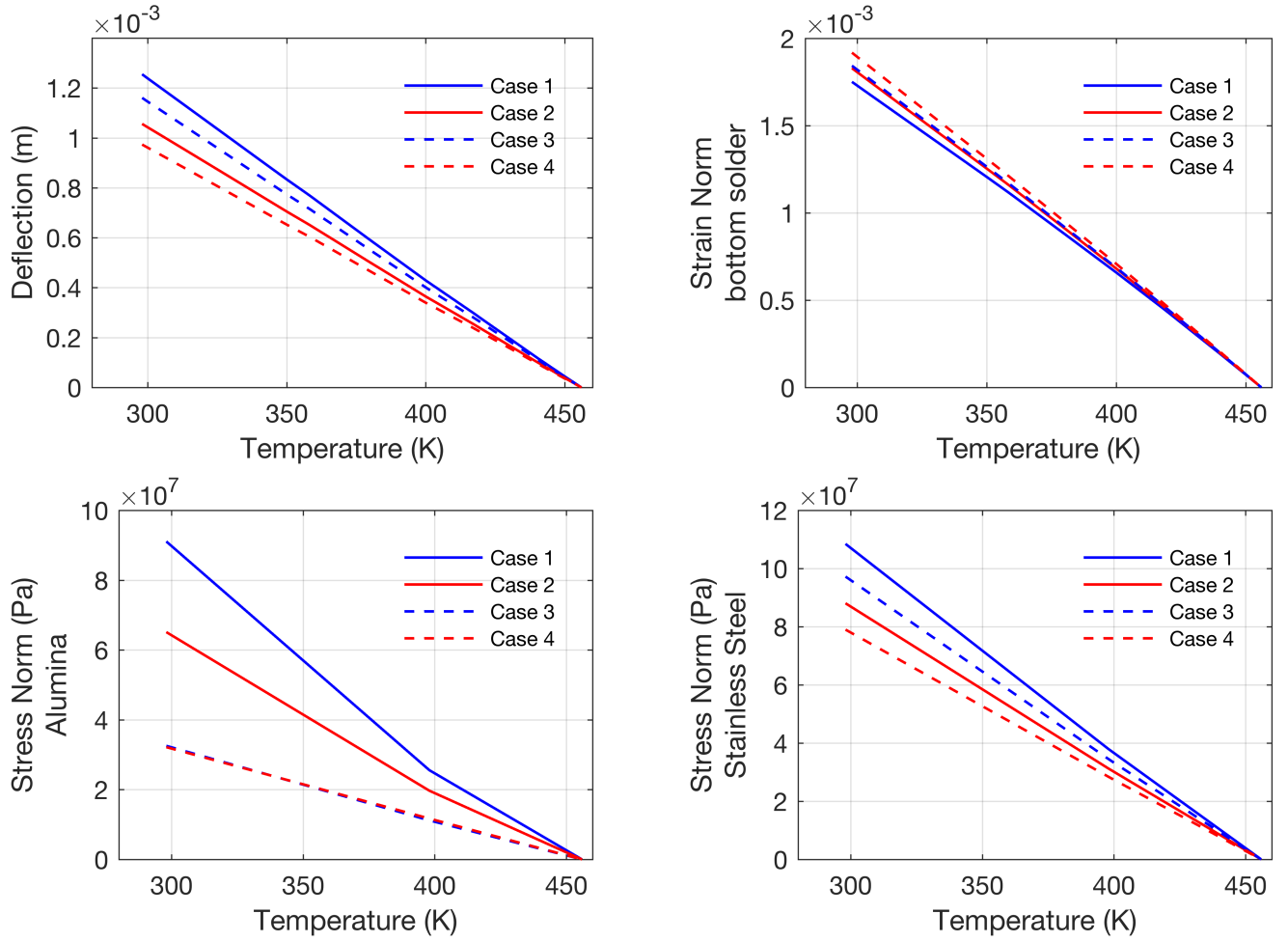


Figure 4: Problem A: Displaying the temperature dependence of strain magnitude in the bottom solder layer, stress magnitude in the Alumina and Stainless Steel and deflection.

and Case 3 and 4 with $m = 2$ is on the right. The deflection versus temperature, the strain magnitude in the bottom solder versus temperature, the stress magnitude in each i layer at $T = 298$, and the boundary stress versus thickness at $T = 298$ were plotted.

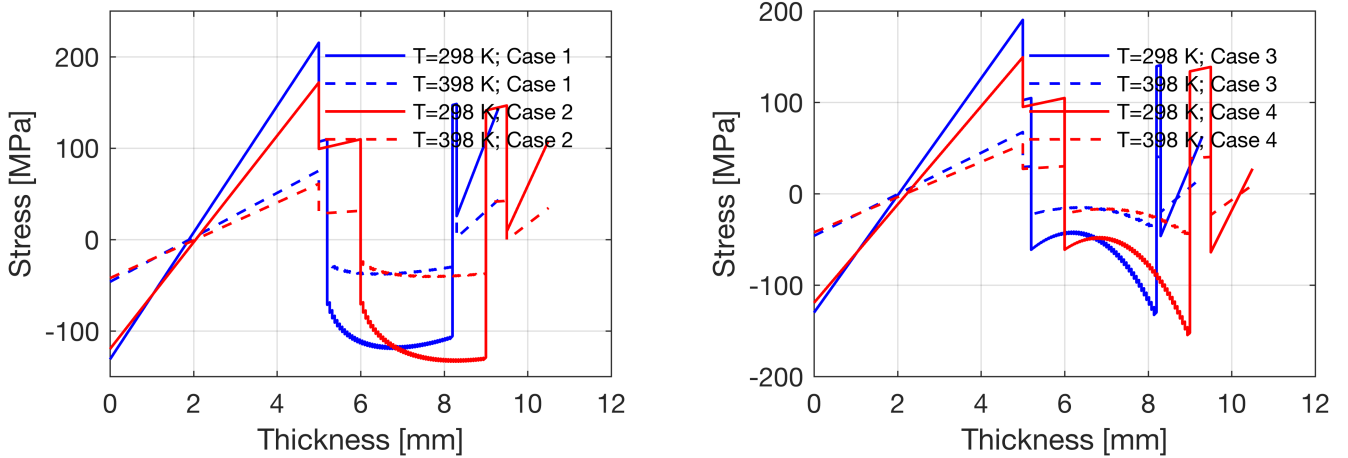


Figure 5: Problem A: Displaying boundary stress versus thickness for all cases.

Based on Figure 5 it can be seen that the thicker the solder the lower the stress and deflection. It is also seen that with $m = 0.25$, meaning that there is more TiG₂, there is less stress and deflection in the gradient layer. The conclusions from this test show that in order to optimize the stress and deflection increasing the solder thickness and decreasing m is best.

Problem B) looked at a three layered material with a $T_{ref} = 295$ K, a $T_{max} = 400$ K and a $T_{min} = 220$ K.

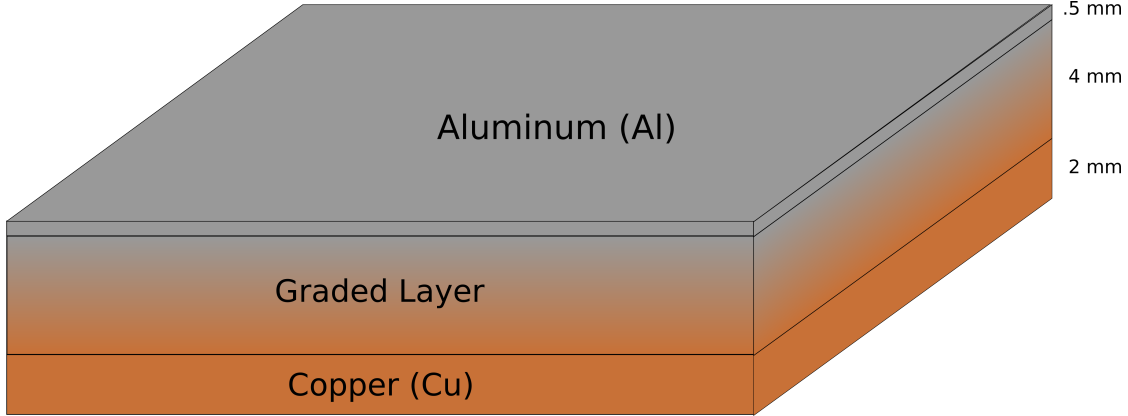


Figure 6: A picture of the set up for problem B.

Aluminum $z = 0.5$ mm	Aluminum $z = 0.5$ mm	Aluminum $z = 0.5$ mm
Aluminum gradation	Aluminum gradation	Aluminum gradation
Copper $z = 4$ mm	Copper $z = 4$ mm	Copper $z = 4$ mm
$n = 50$	$n = 50$	$n = 50$
$m = 0.25$	$m = 1.0$	$m = 4.0$
Copper $z = 2$ mm	Copper $z = 2$ mm	Copper $z = 2$ mm

Table 3: The different cases looked at for problem B.

The variation of the gradient exponent m was studied. The $m < 1$ means the gradient material moved faster to pure Al, a $m = 1$ means taht it was a linear step from Cu to Al and a $m > 1$ means it took longer to get to pure Al. The boundary stress versus thickness at $T = 220$ K, the stress magnitude in each layer i at $T = 200$ K and the deflection versus temperature were plotted to compare the different m values.

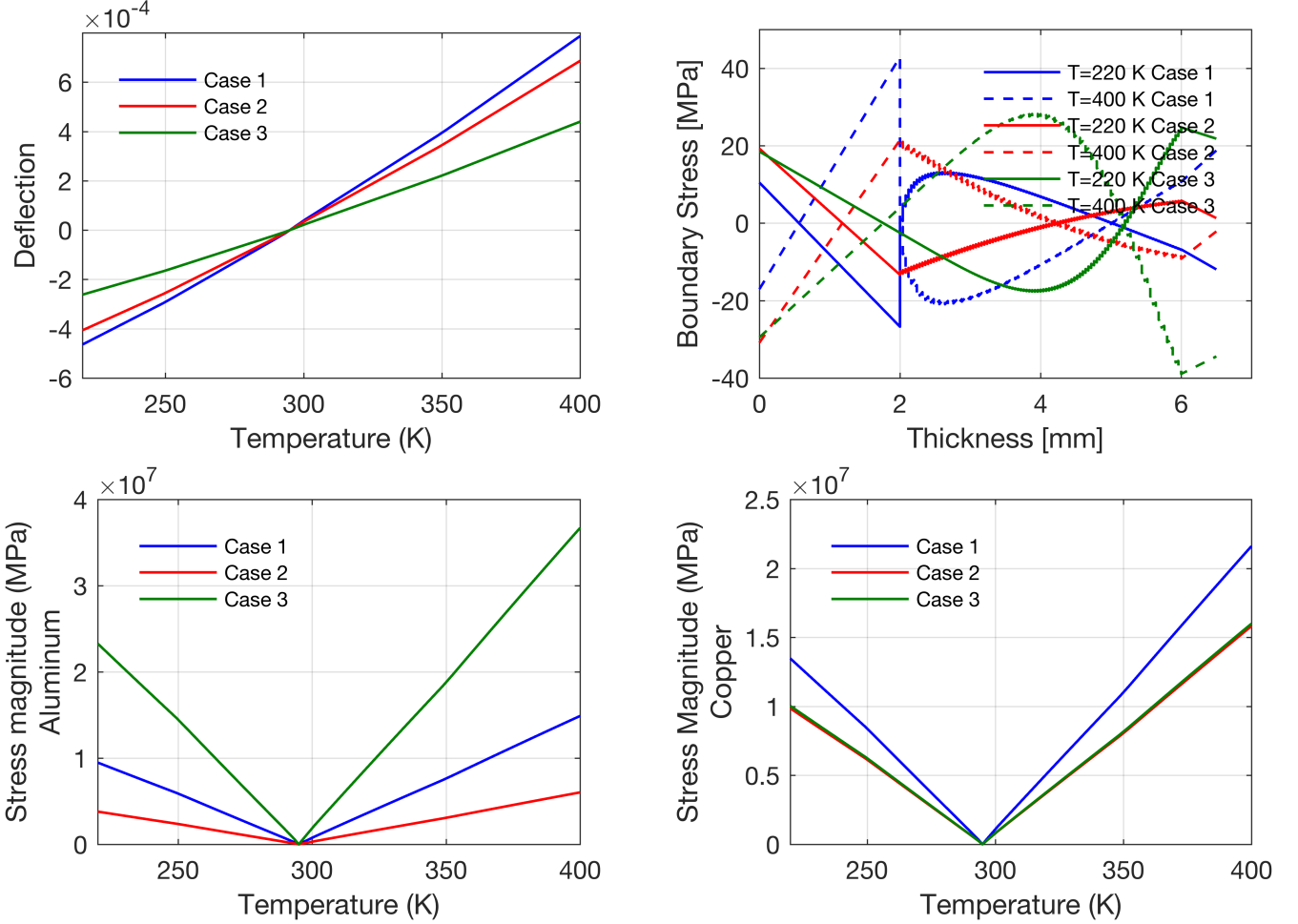


Figure 7: Problem B: Displaying the temperature dependence of deflection, the magnitude stress in the Al layer, the magnitude of stress in the Cu layer and the boundary stress versus thickness at two temperatures.

Based on Figure 7 it can be seen that $m > 1$, meaning having more Cu, leads to a lower deflection but has a larger boundary and magnitude stress. The case when $m < 1$, meaning more Al, has the lowest deflection but still the second highest boundary and magnitude stress. Finally, when $m = 1$ we have the lowest stress and the second lowest deflection. In this case if you are trying to optimize to stress and deflection $m = 1$ would be best but this is very application dependent.

The final problem, Problem C) looked at how the number of layers would effect the stress and deflection. The structure of interest is a material with a varying amount of alternating layer pairs.

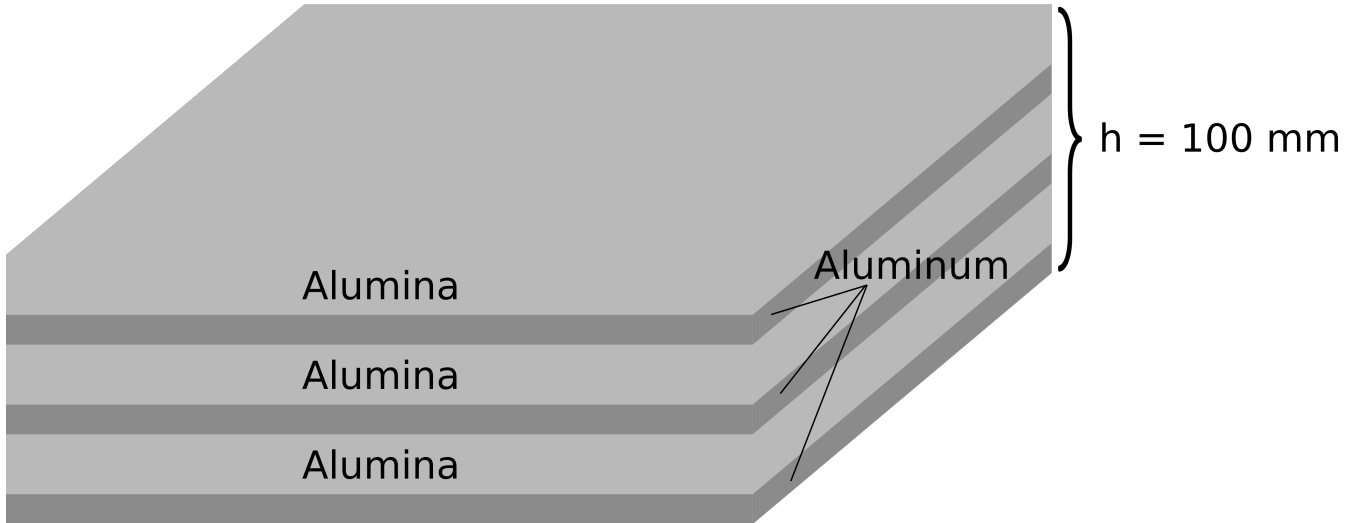


Figure 8: Depiction of the setup for problem C.

We imagine a setup

$$N_{\text{pairs}} = \begin{cases} \text{Material}_1 \\ \text{Material}_2 \\ \text{Material}_1 \\ \text{Material}_2 \\ \vdots \end{cases}$$

Denoting the thickness of each material in the pair by h_1 and h_2 respectively then the total thickness of the structure is $h = N(h_1 + h_2)$. The $T_{ref} = 600$ K, $T_{max} = 800$ K and $T_{min} = 298$ K. We let the number of layers vary between 2 and 40.

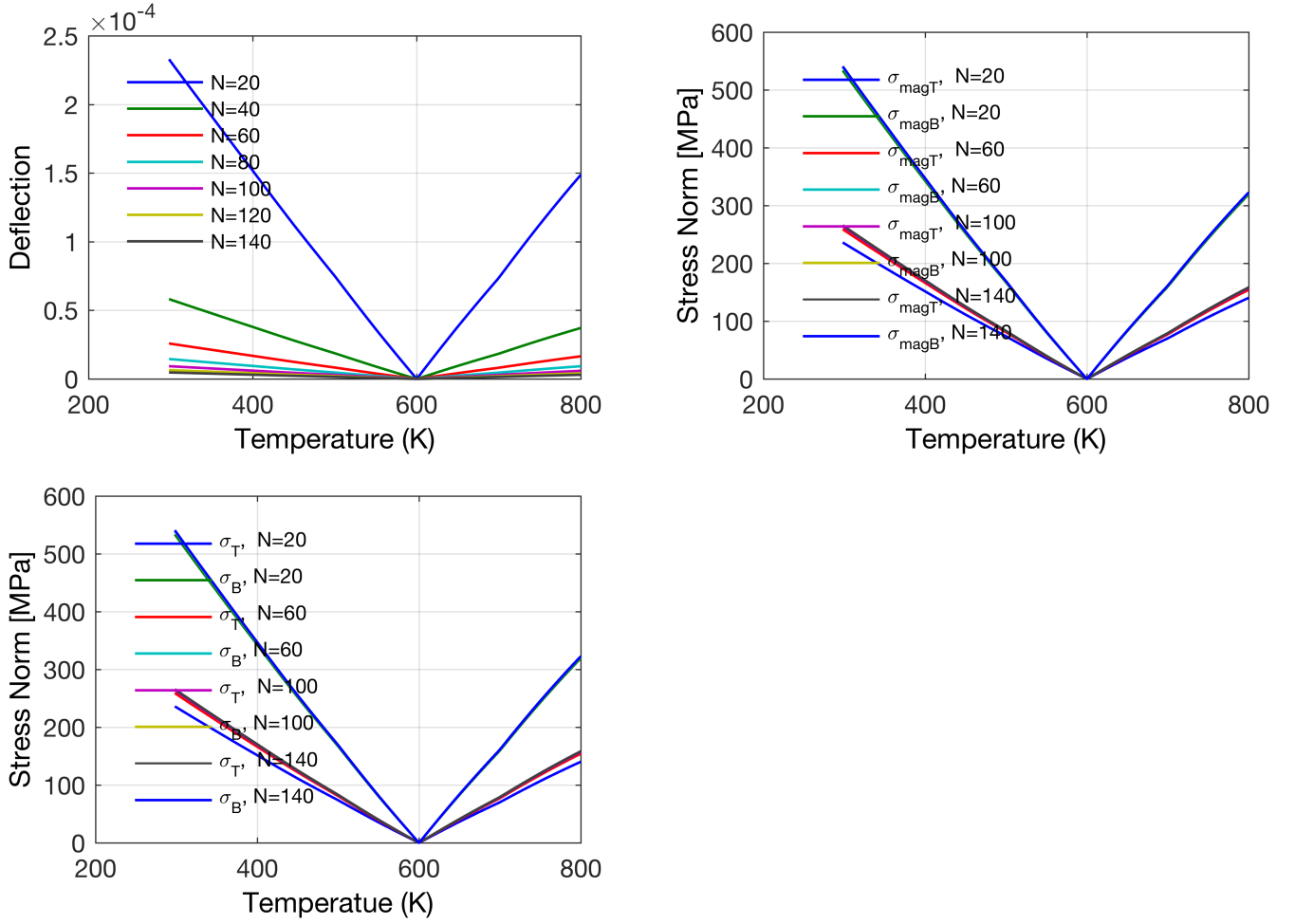


Figure 9: Problem C: Displaying the effect of changing the number of layers.

From Figure 9 it is seen that increasing the number of layers decreased the deflection and stress. At some point the results begin to converge even with the increase in layers. The minimum deflection solution was largely independent of thickness ratio. Based on our above results, a more thorough sensitivity testing of the effects of each variable on the output was performed.

3.2 Sensitivity

To begin the sensitivity testing, we first tried an analytical study. We considered every parameter with respect to temperature. But based on the complexity of the equations we decided to look at two cases instead.

3.2.1 Analytical Sensitivity Testing

In what follows, we consider different cases to demonstrate the difficulties of Analytical sensitivity analysis. So we first consider the general case and try to break down to simpler cases but at the end analytical analysis is very demanding.

For the general case we take the derivative of σ_i with respect to temperature T . Using $\dot{1}$ and $\dot{2}$ we get the following first order differential equation with respect to the temperature which can be solved by the integration factor method to obtain:

$$f(T) \frac{\partial \sigma_i}{\partial T} + g(T) \sigma_i = h(T), \quad (30)$$

where

$$f(T) = \frac{F}{\bar{E}_i} \quad (31)$$

$$g(T) = \left(\frac{F'}{\bar{E}_i} - \frac{F\bar{E}'_i}{\bar{E}_i^2} \right) \quad (32)$$

$$h(T) = [4(A_3 - B_3)'(C_1 - D_1) + 4(A_3 - B_3)(C_1 - D_1)' - 3(A_2 - B_2)(C_2 - D_2)' - 3(A_2 - B_2)'(C_2 - D_2)] + 6z[(A_1 - B_1)'(C_2 - D_2) + (A_1 - B_1)(C_2 - D_2)' - (A_2 - B_2)'(C_1 - D_1) - (A_2 - B_2)(C_1 - D_1)'] - (F\epsilon_{th})'.$$

Thererfore we obtain:

$$\frac{\partial \sigma_i}{\partial T} = \frac{\frac{h(T)}{\sigma_i} - g(T)}{f(T)}. \quad (33)$$

Now we consider the case where \bar{E}_i is independent of change in T , i.e. $\frac{\partial \bar{E}_i}{\partial T} = 0$. Then we have

$$\frac{\partial A_k}{\partial T} = 0 = \frac{\partial B_k}{\partial T}, \quad \frac{\partial C_k}{\partial T} = \sum_{i=1}^N \bar{E}_i \epsilon_i^{th'} z_i^k, \quad \frac{\partial D_k}{\partial T} = \sum_{i=1}^N \bar{E}_i \epsilon_i^{th'} z_{i-1}^k, \quad \frac{\partial F}{\partial T} = 0, \quad g(T) = 0. \quad (34)$$

which yields

$$f(T) \frac{\partial \sigma_i}{\partial T} = [4(A_3 - B_3)(C_1 - D_1)' - 3(A_2 - B_2)(C_2 - D_2)'] - F\epsilon_i^{th'} + 6z[(A_1 - B_1)(C_2 - D_2)' - (A_2 - B_2)(C_1 - D_1)'].$$

$$\frac{\frac{\partial \sigma_i}{\partial T}}{\sigma_i} = \frac{[4(A_3 - B_3)(C_1 - D_1)' - 3(A_2 - B_2)(C_2 - D_2)'] - F\epsilon_i^{th'} + 6z[(A_1 - B_1)(C_2 - D_2)' - (A_2 - B_2)(C_1 - D_1)']}{[[4(A_3 - B_3)(C_1 - D_1) - 3(A_2 - B_2)(C_2 - D_2)] - F\epsilon_i^{th} + 6z[(A_1 - B_1)(C_2 - D_2) - (A_2 - B_2)(C_1 - D_1)]]}$$

Lastly we take the derivative w.r.t the thermal strain ϵ_{th} . Due to the fact $\frac{\partial \bar{E}_i}{\partial \epsilon_j^{th}} = 0$ we obtain

$$\frac{\partial A_k}{\partial \epsilon_j^{th}} = 0 = \frac{\partial B_k}{\partial \epsilon_j^{th}}, \quad \frac{\partial C_k}{\partial \epsilon_j^{th}} = \sum_{i=1}^N \bar{E}_i z_i^k \delta_{ij} = \bar{E}_j z_j^k, \quad \frac{\partial D_k}{\partial \epsilon_j^{th}} = \sum_{i=1}^N \bar{E}_i z_{i-1}^k \delta_{ij} = \bar{E}_j z_{j-1}^k, \quad \frac{\partial F}{\partial \epsilon_j^{th}} = 0, \quad g(T) = 0.$$

Then we have

$$\begin{aligned} \frac{F}{\bar{E}_i} \frac{\partial \sigma_i}{\partial \epsilon_j^{th}} &= [4(A_3 - B_3)(C_1 - D_1)'_{th} - 3(A_2 - B_2)(C_2 - D_2)'_{th}] - F \frac{\partial \epsilon_i^{th}}{\partial \epsilon_j^{th}} + 6z[(A_1 - B_1)(C_2 - D_2)'_{th} - (A_2 - B_2)(C_1 - D_1)'_{th}] \\ &= [\bar{E}_j [4(A_3 - B_3)(z_j - z_{j-1}) - 3(A_2 - B_2)(z_j^2 - z_{j-1}^2)] - F \frac{\partial \epsilon_i^{th}}{\partial \epsilon_j^{th}} + 6z[(A_1 - B_1)(z_j^2 - z_{j-1}^2) - (A_2 - B_2)(z_j - z_{j-1})]] \\ \frac{\frac{\partial \sigma_i}{\partial \epsilon_j^{th}}}{\sigma_i} &= \frac{\bar{E}_j [4(A_3 - B_3)(z_j - z_{j-1}) - 3(A_2 - B_2)(z_j^2 - z_{j-1}^2)] - F \frac{\partial \epsilon_i^{th}}{\partial \epsilon_j^{th}} + 6z[(A_1 - B_1)(z_j^2 - z_{j-1}^2) - (A_2 - B_2)(z_j - z_{j-1})]}{[[4(A_3 - B_3)(C_1 - D_1) - 3(A_2 - B_2)(C_2 - D_2)] - F\epsilon_i^{th} + 6z[(A_1 - B_1)(C_2 - D_2) - (A_2 - B_2)(C_1 - D_1)]]} \end{aligned} \quad (35)$$

Based on the derivations in equation 33 we found that even an analytical study of the E_i independent of temperature is cumbersome. Due to the difficulty of analytically studying the sensitivity we numerically studied the sensitivity of the variables through Problem A and B.

3.2.2 Sensitivity Analysis For Problem A

We test the sensitivity of certain quantities to certain parameters in problem A. The quantities of interest (QOI) are the stress in alumina, the strain in solder 1, the strain in solder 2, and the deflection. The varied parameters are the thickness of solder 1, the thickness of solder 2, the exponent of gradation, the Young's modulus of stainless steel, the Poisson's ratio of stainless steel, and the thermal strain of stainless steel. These are listed in Table 4. Each parameter is varied while the others are kept fixed. The reference value for the varying parameter and the value of the fixed parameters are those given in Problem A. Except for the exponent of gradation, all parameters are varied within 50%. The exponent of gradation is varied within a factor of five. The QOI are then calculated for each parameter value.

Quantities of Interest		Varied Parameters	
σ_N	δ	z_{s1}	E_1
ε_{s1}		z_{s2}	ν_1
ε_{s2}		m	ε_1^{th}

Table 4: List of quantities of interest and varied parameters for sensitivity analysis in Problem A.

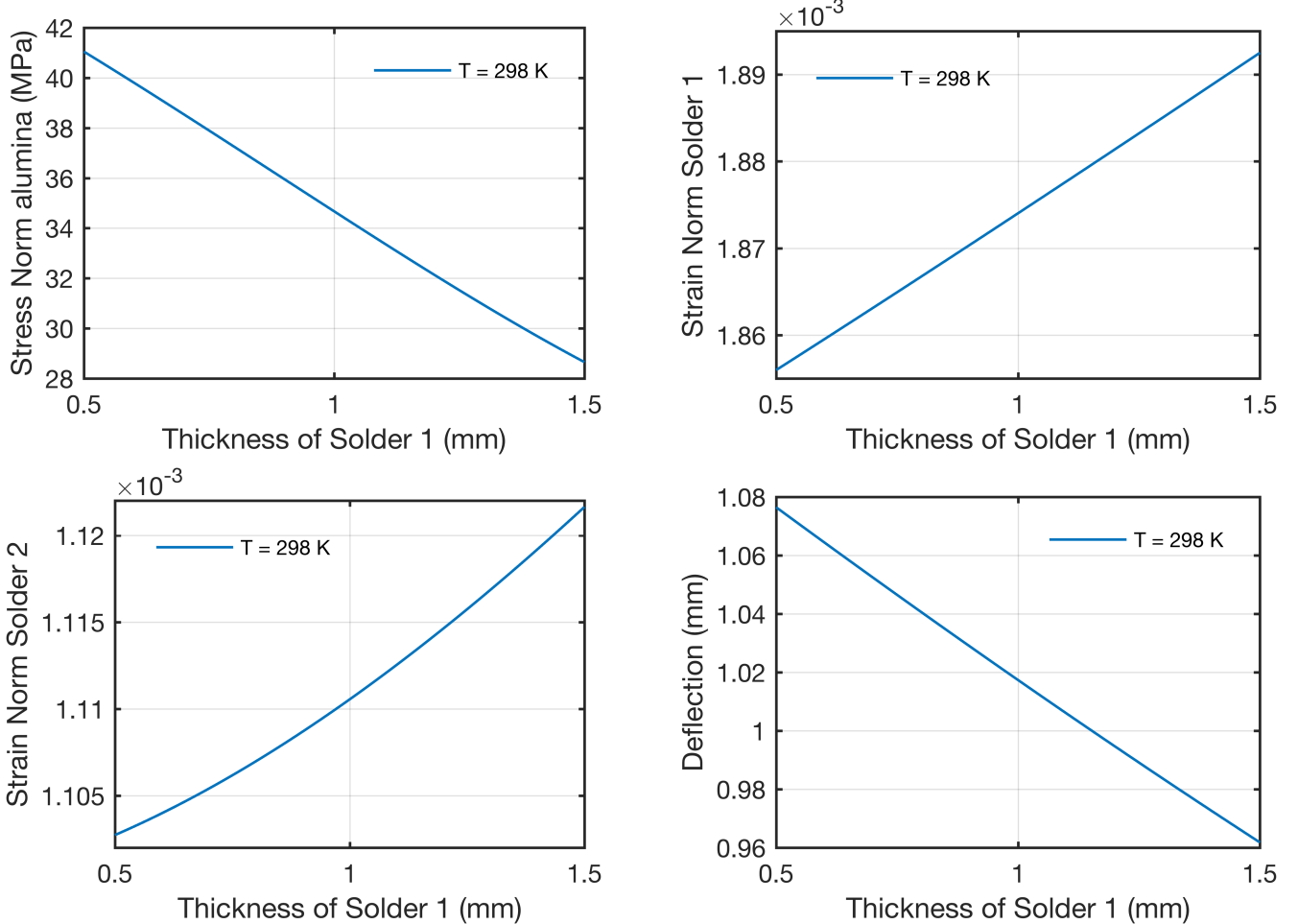


Figure 10: Plots of quantities of interest versus thickness of solder 1. The y -axis is the actual value of the QOI, and the x -axis is the actual value of the thickness of solder 1.

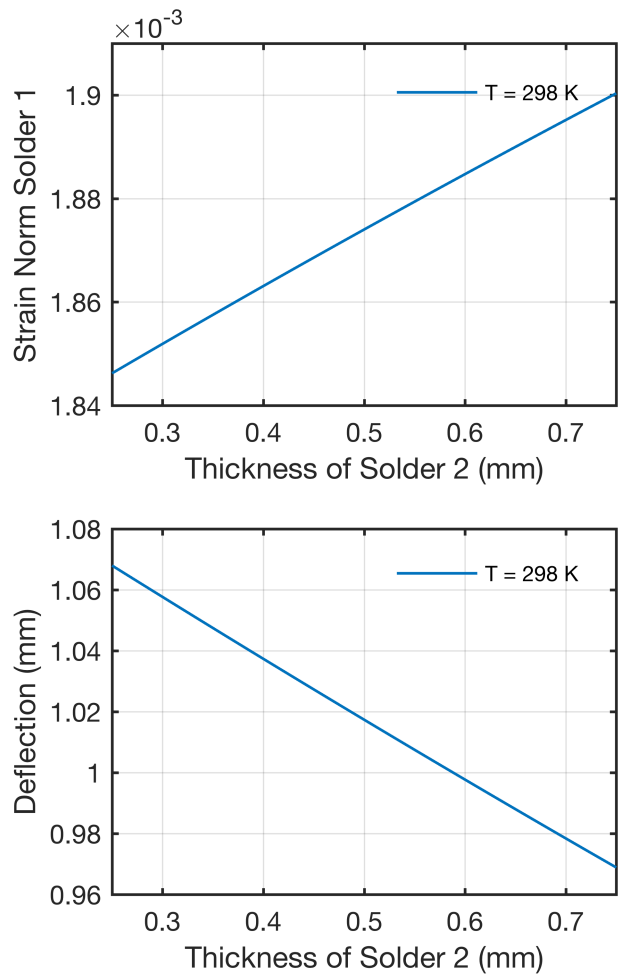
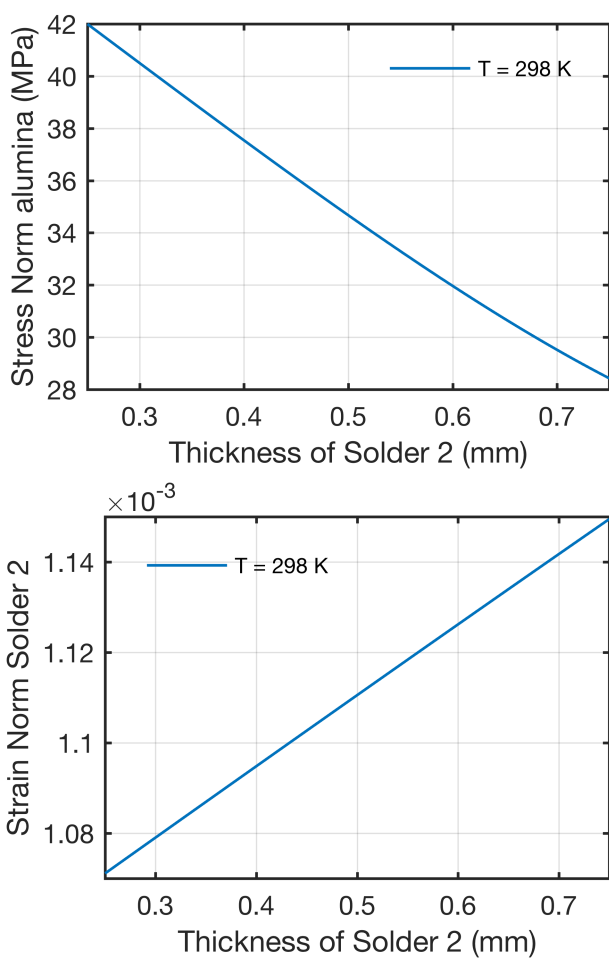


Figure 11: Plots of quantities of interest versus thickness of solder 2. The y -axis is the actual value of the QOI, and the x -axis is the actual value of the thickness of solder 1.

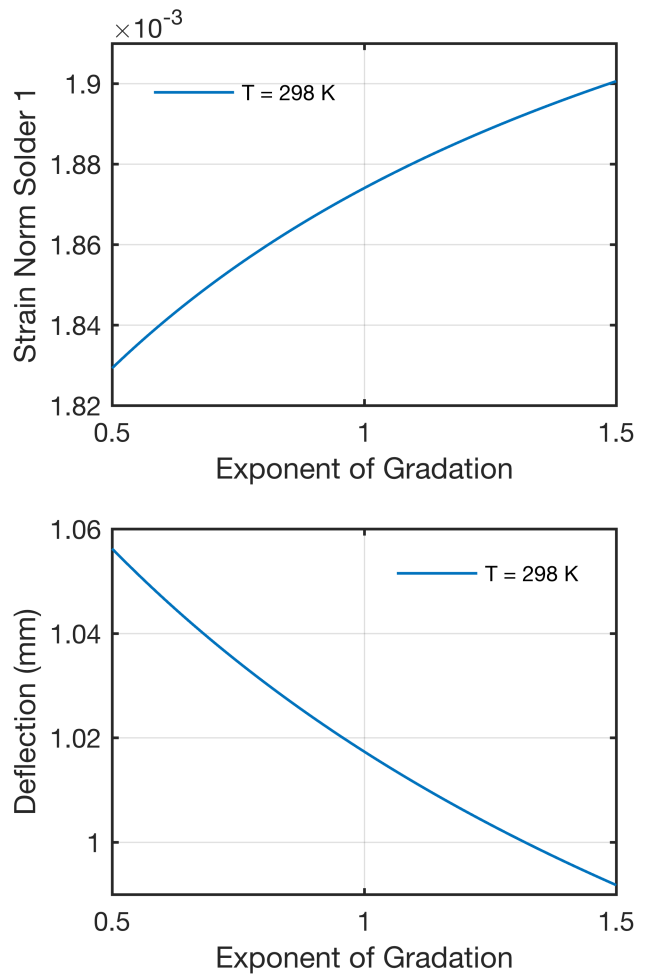
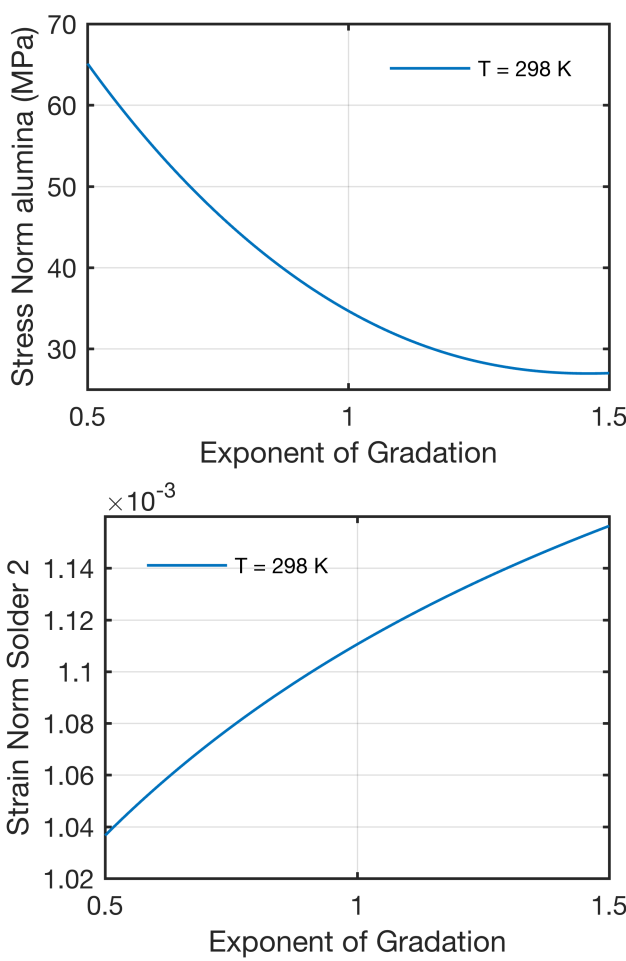


Figure 12: Plots of quantities of interest versus exponent of gradation. The *y*-axis is the actual value of the QOI, and the *x*-axis is the actual value of the exponent of gradation.

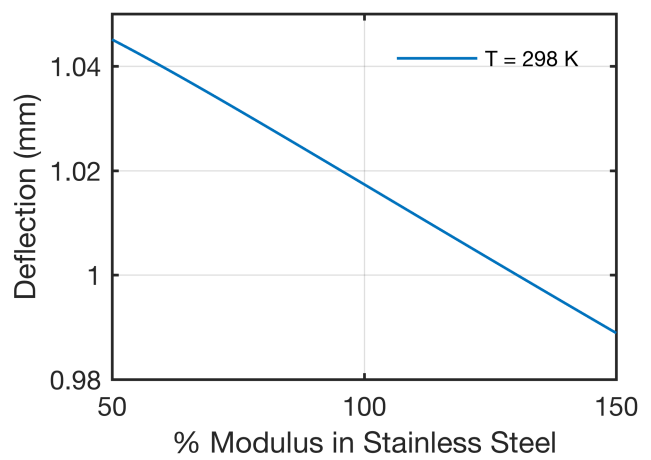
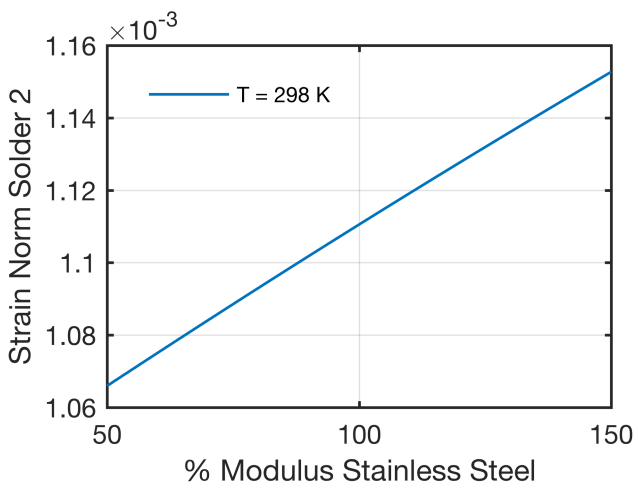
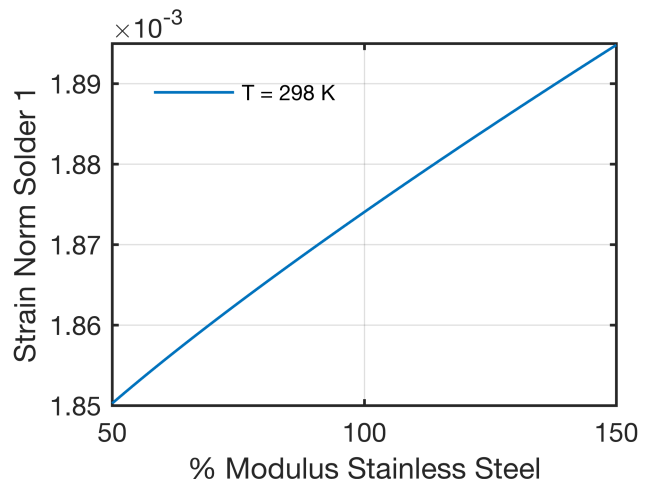
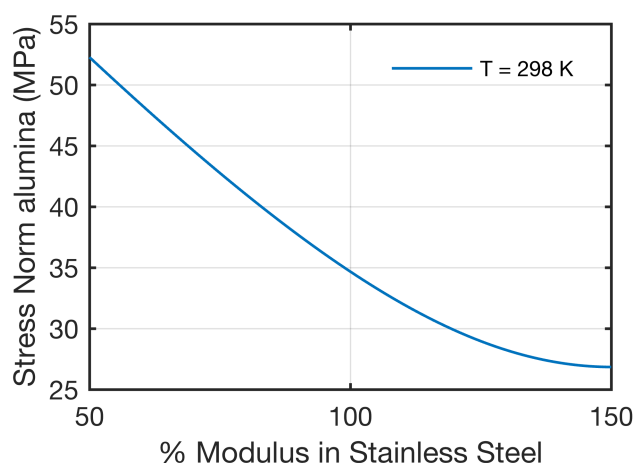


Figure 13: Plots of quantities of interest versus Young's modulus of stainless steel. The *y*-axis is the actual value of the QOI, and the *x*-axis is the percent of Young's modulus of stainless steel.

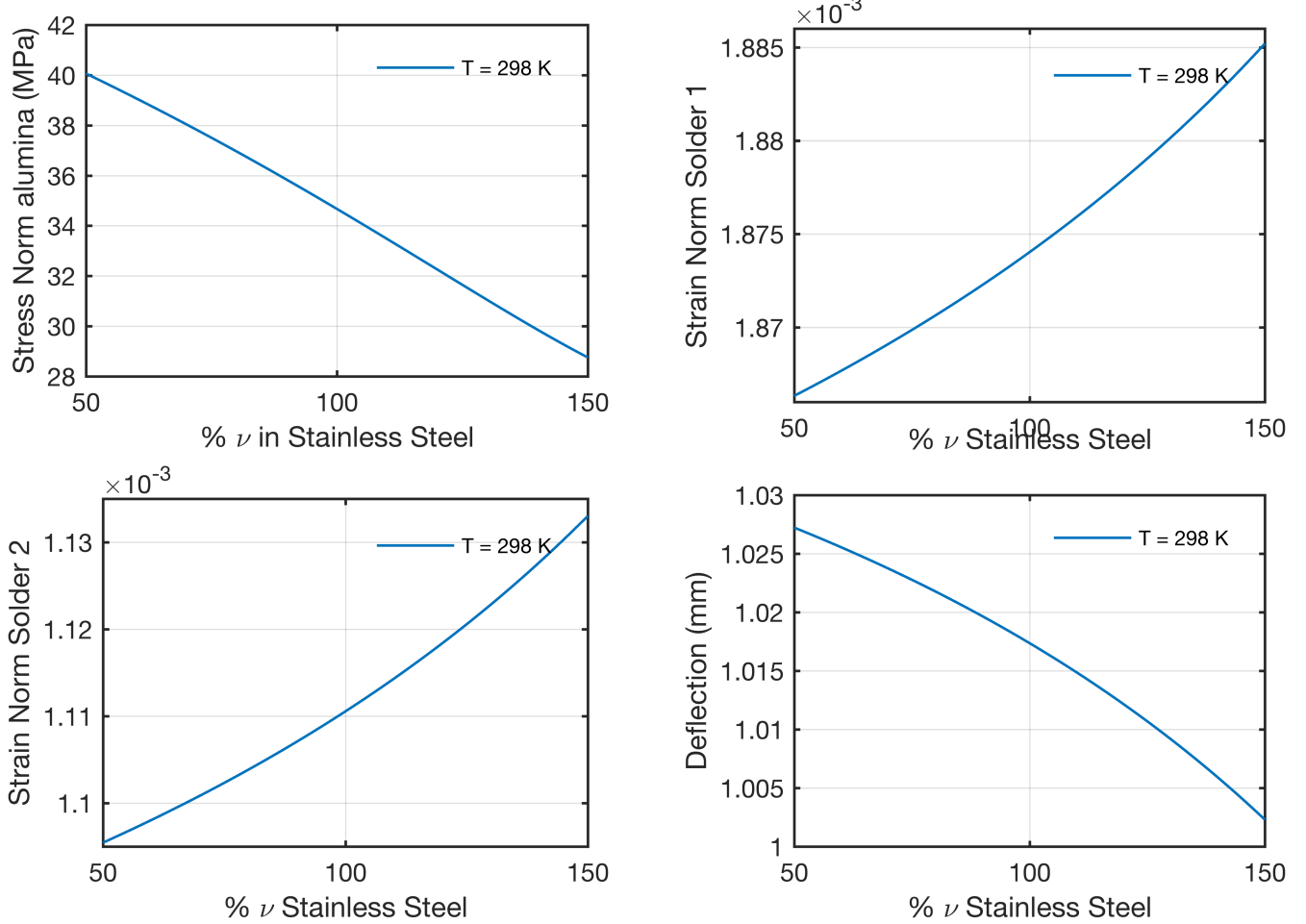


Figure 14: Plots of quantities of interest versus Poisson's ratio of stainless steel. The y -axis is the actual value of the QOI, and the x -axis is the percent of Poisson's ratio of stainless steel.

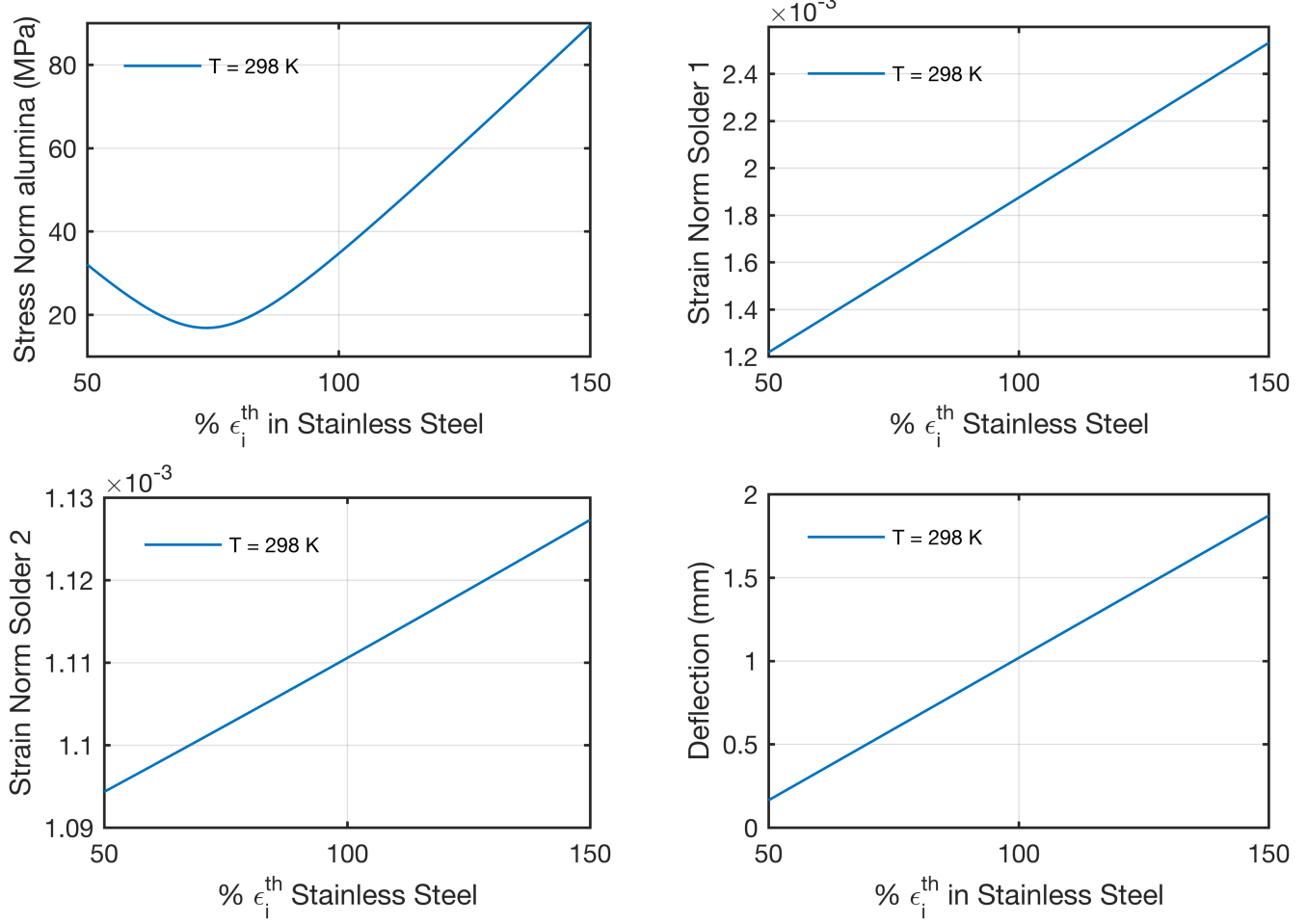


Figure 15: Plots of quantities of interest versus thermal strain of stainless steel. The y -axis is the actual value of the QOI, and the x -axis is the percent of thermal strain of stainless steel.

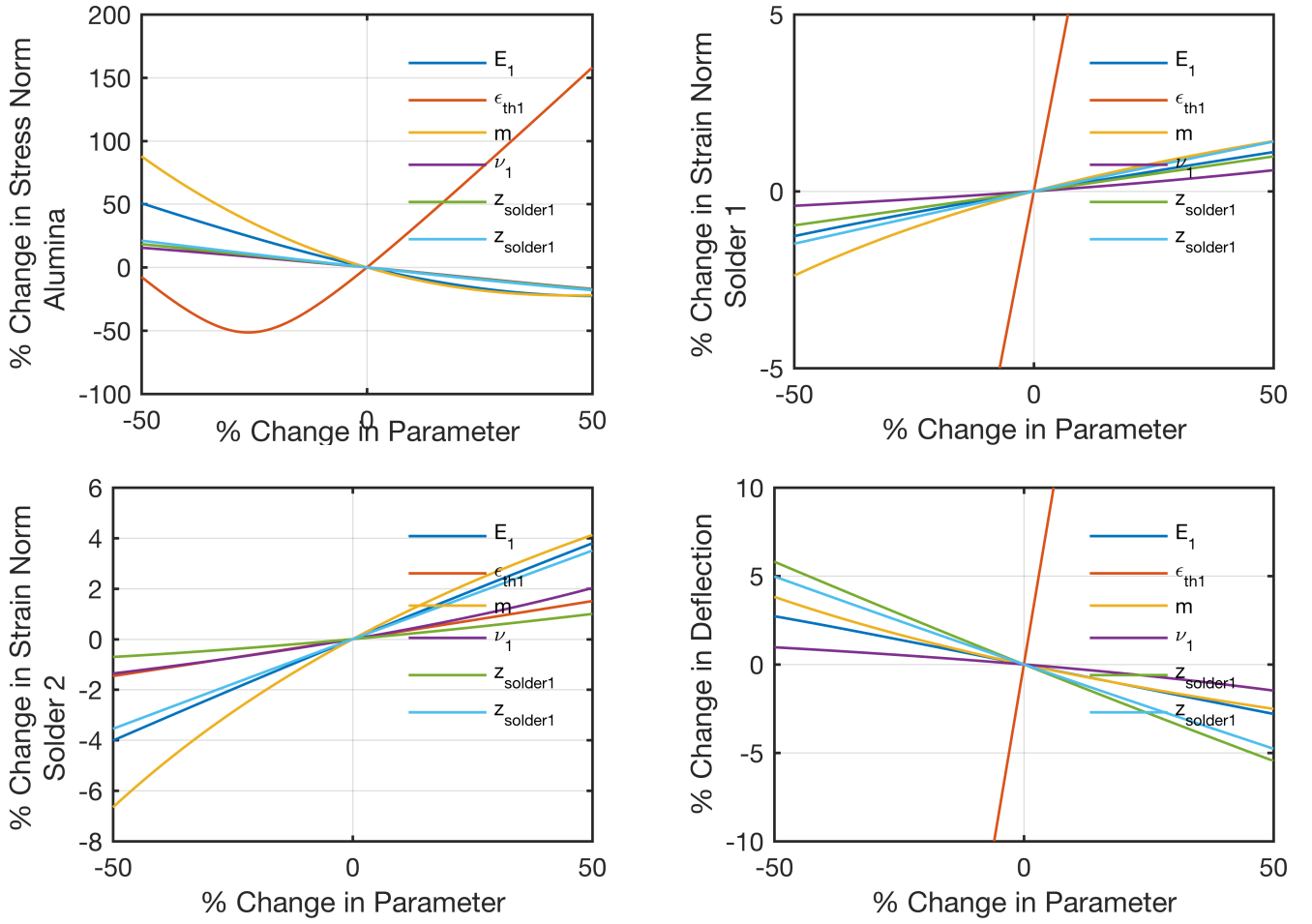


Figure 16: Sensitivity plots. The y -axis is the percent change in the QOI, and the x -axis is the percent change in the varied parameters.

Figures 10 - 15 show the individual results of (QOI) versus (parameter value), whereas Figure 16 shows the collective results in a sensitivity plot of (percent change in QOI) versus (percent change in parameter). These results show that a QOI can be very sensitive to a certain parameter and not others. For instance, strain in solder 1 and deflection vary much more rapidly with respect to thermal strain of stainless steel than with other parameters. These results also show that which parameter has the greatest effect depends on the QOI. Strain in solder 2 is most sensitive to gradation exponent, while the other QOI are most sensitive to thermal strain of stainless steel. Another observation is that certain QOI respond nonlinearly to changes in parameters. Most notably, stress in alumina varies nonlinearly between a 40% and 10% reduction in thermal strain of stainless steel. Such analysis can help streamline experimental design for desired effects.

3.2.3 Sensitivity Analysis For Problem B

In this section we do the sensitivity analysis for problem B. We compute the L^2 norm and deflection while changing the following parameters in the Copper:

- Exponent of Gradation m
- Young's Modulus E
- Possion's Ratio ν

- Thermal Strain ϵ_{th}
- Thickness of graded layers between Aluminum and Copper

Case 1) Sensitivity analysis of Exponent: The exponent varied in the interval of $[\frac{m}{5}, 5m]$.

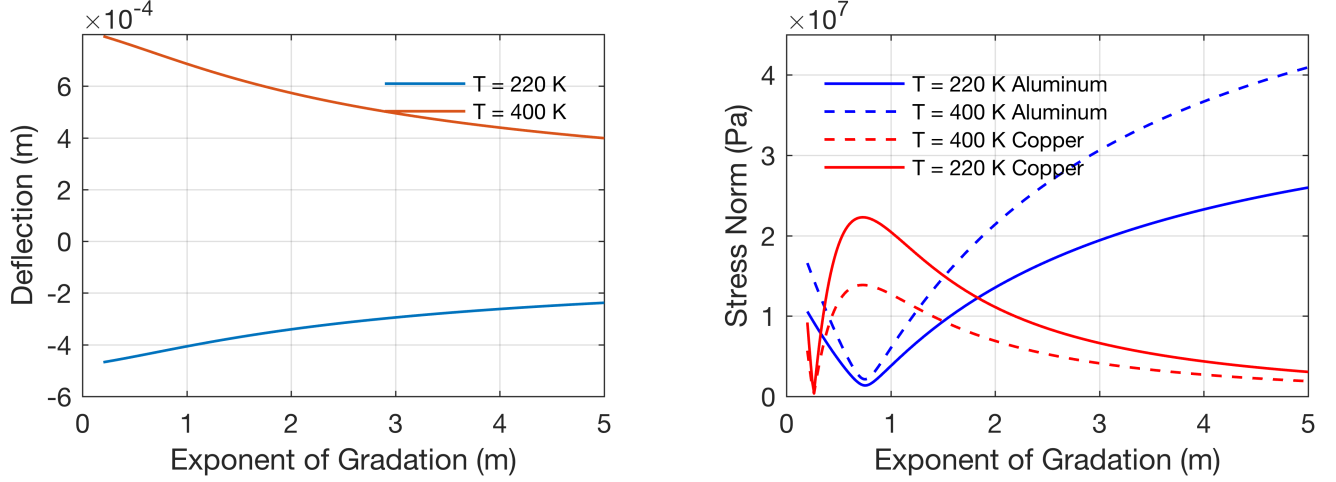


Figure 17: Sensitivity plots of the gradient exponent m .

The sensitivity analysis in Figure 17 shows that varying the exponent m leads to a nonlinear behaviour of L^2 norm of Aluminum and Copper, and deflection. The L^2 norm of Aluminum reaches a minimum around $m = 0.744$ while L^2 norm of Copper reaches its maximum. The deflection also shows nonlinear behaviour.

Case 2) Sensitivity analysis of Young's Modulus: The Young's Modulus E varies in the interval $[0.5E, 1.5E]$.

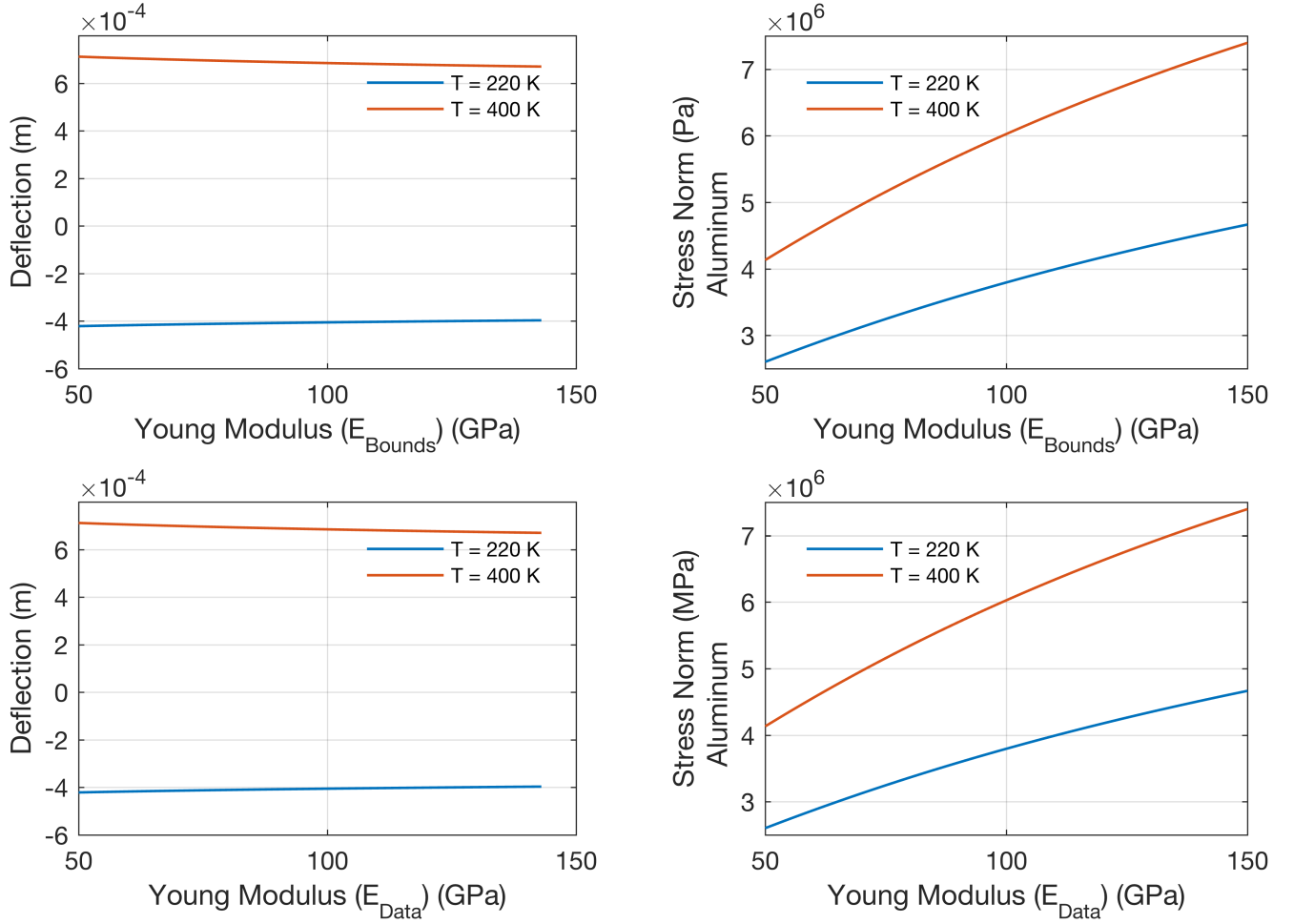


Figure 18: Sensitivity plots of the Young's modulus.

The sensitivity analysis shown in Figure 18 that as the Young's Modulus E increases for Copper and the L^2 norm of Aluminum increases. However the deflection shows an almost linear behaviour.

Case 3) Sensitivity analysis of Possion's Ratio: The Possion's Ratio ν varies in the interval $[0.5\nu, 1.5\nu]$.

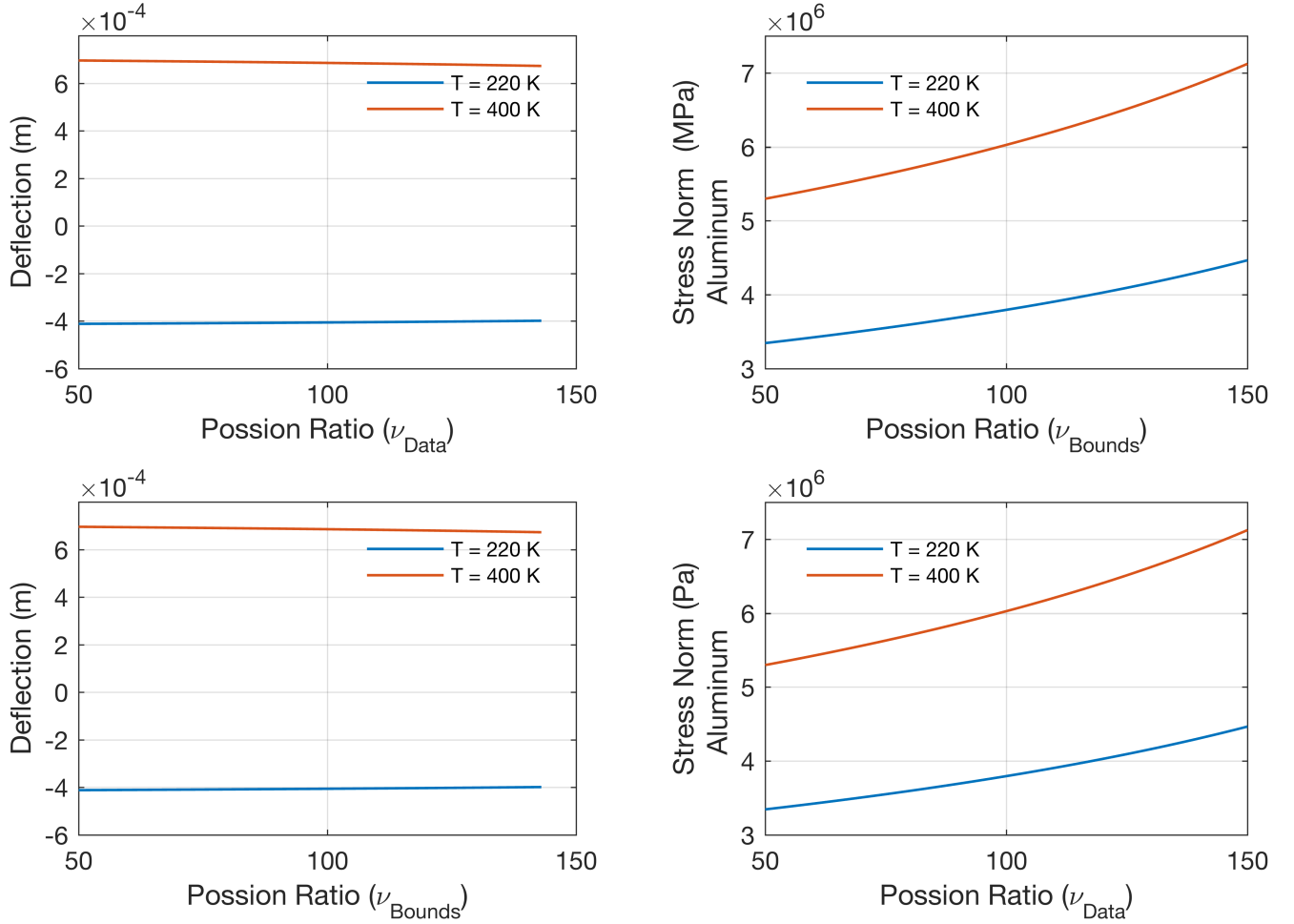


Figure 19: Sensitivity plots of the Poisson's Ratio.

As it can be seen in the Figure 19 the L^2 norm increases as the Possion's Ratio ν increases. The sensitivity analysis of ν is done with the constraint of $0 < \nu < 0.5$ is satisfied. For deflection we see similar behaviour as the case for Young's Modulus.

Case 4) Sensitivity analysis of Thermal Strain: The Thermal Strain ϵ_{th} varies in the interval $[0.5\epsilon_{th}, 1.5\epsilon_{th}]$.

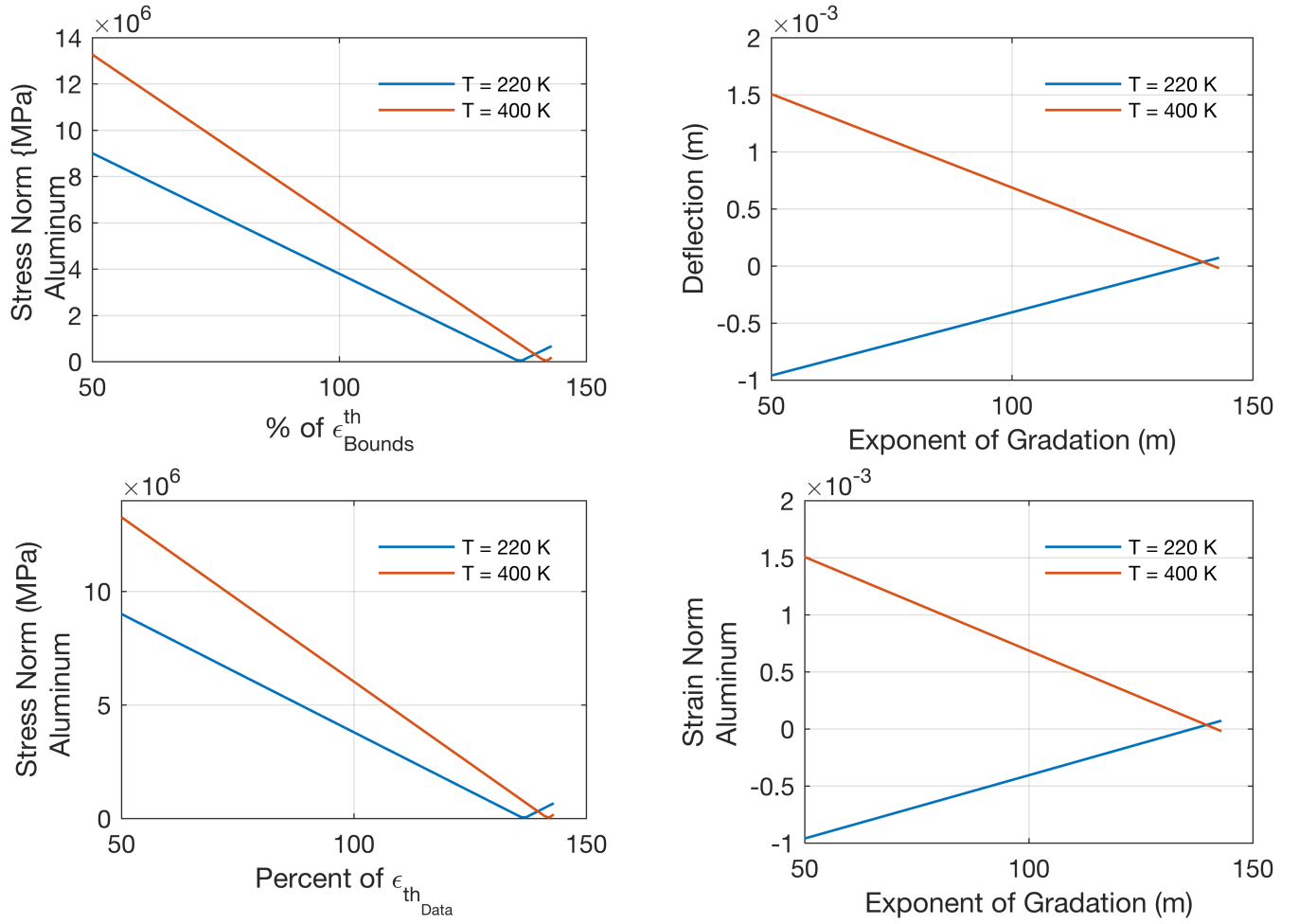


Figure 20: Sensitivity plots of the thermal strain.

From Figure 20 the sensitivity analysis shows linear decrease in the L^2 norm of Aluminum as the thermal strain increases.

Case 5) Sensitivity analysis of Thickness of graded layers:

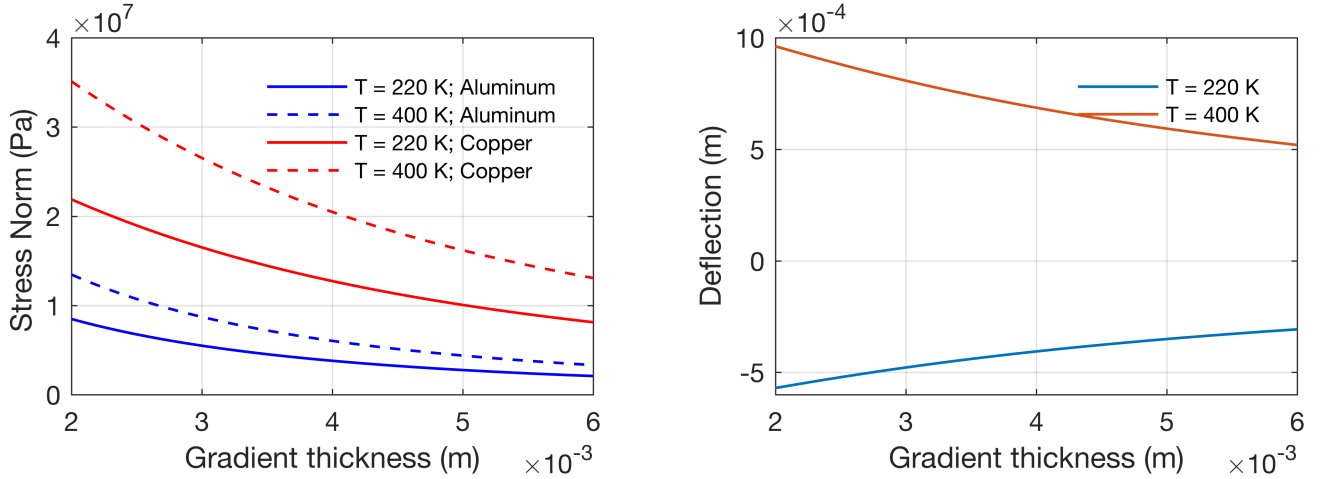


Figure 21: Sensitivity plots of the gradient thickness.

Figure 21 shows the the L^2 norm of Aluminum and Copper decrease nonlinearly as the graded thickness increases.

3.3 Optimization

Seeing how the sensitivity of a parameter is greatly dependent on the quantity of interest and the may not be linear we looked at how we could optimize these parameters based on the original problems.

3.3.1 Optimization of Problem A

For our optimization, we started by focusing on the Problem A) decribed in the forward model subsection. We explore two distinct objective functions; stress in the insulating alumina layer, and total deflection. In application, we would likely apply some linear combination of these, but for illustrative purposes we will examine them separately.

We calculate the stress (and deflection) over a range of temperatures. We then have a two variable function $\sigma(z, T)$ (in the case of stress) as per (6), from which we must compute a scalar “norm”. In our case, we take the maximum in space and an L_1 average in temperature to obtain this

$$\|\sigma\| \equiv \int_{T_i}^{T_f} \max_{z \in Al_2O_3} \sigma(z, T) dT. \quad (36)$$

Computationally, the integral is approximated by a first-order discretization method. We allow the two thicknesses to range between 0.05 and 1 mm.

1) Varying Solder Thickness

We first examine an optimization scenario based on the first scenario described above, but allow the thickness of the solder to vary.

A plot of the stress objective (36) versus solder thickness is shown in Figure 22. We see a minimum stress occurs when the thickness of the solder connecting the alumina to the Ti/invar layer is 0.59 mm, and the solder connecting the Ti/invar to the stainless steel is at the maximum value of 1 mm.

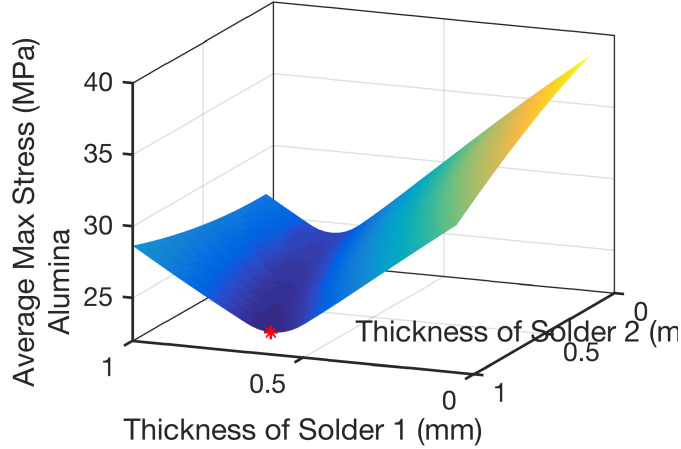


Figure 22: Solder thickness versus temperature-averaged maximum stress in alumina layer. The optimal value is highlighted, and occurs at approximately (.59, 1).

This optimum is calculated using MATLAB's `fmincon` function. The well-behaved nature of the objective surface (shown in Figure 22) allows `fmincon` to run quickly and without complication using its default settings.

When we employ deflection as our objective (temperature averaged similar to (36)) we find that the minimum deflection occurs on the boundary of our optimization region, that is to say when both solders have the maximum thickness of 1 mm. This is unsurprising, since increased thickness would intuitively decrease the deflection. The objective function plotted against solder thickness (not shown) is approximately planar, and increases with decreasing thickness.

Since the objective surfaces are straightforward, one can readily guess the behavior if we are to use a linear combination of the two surfaces. To wit, the optimal value for the first solder layer (alumina to Ti/invar) is between 0.59 and 1 (depending on the coefficients of the linear combination in our objective function), and the optimal value of the second solder layer remains 1 mm.

2) Varying Exponent of Gradation

Now we will examine the effect of varying the exponent of gradation on our various objective functions. That is to say, we will fix the solder thicknesses at 1 mm and allow the exponent m to vary.

Proceeding as before, we first examine a temperature-averaged maximum stress in the alumina. We allow the exponent of gradation to range between $m = 0.1$ and $m = 10$. Figure 23 shows a plot of max average stress against gradation exponent. The optimal value is clearly visible, and is calculated to be approximately $m = 0.76$.

That the optimal exponent is close to 1 indicates that a smooth transition between materials minimizes stress. This fact is balanced with the effect of the different material properties of titanium and invar. Since the exponent is less than 1, the graded material has mean properties closer to invar than titanium. This is unsurprising, since invar undergoes less thermal strain than titanium, that is to say, $\varepsilon_{\text{Invar}}^{\text{th}} < \varepsilon_{\text{Ti}}^{\text{th}}$.

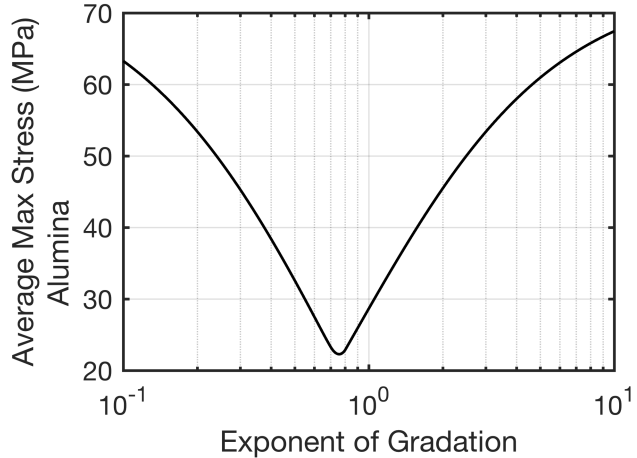


Figure 23: Average max stress against exponent of gradation. Minimum occurs at $m \approx 0.76$.

In the situation where we wish to minimize deformation, we do not obtain an interior minimum. The endpoint $m = 10$ yields minimal deformation, as seen in Figure 24. This indicates that the optimal choice for minimizing deflection is to make the material entirely titanium, as we might expect.

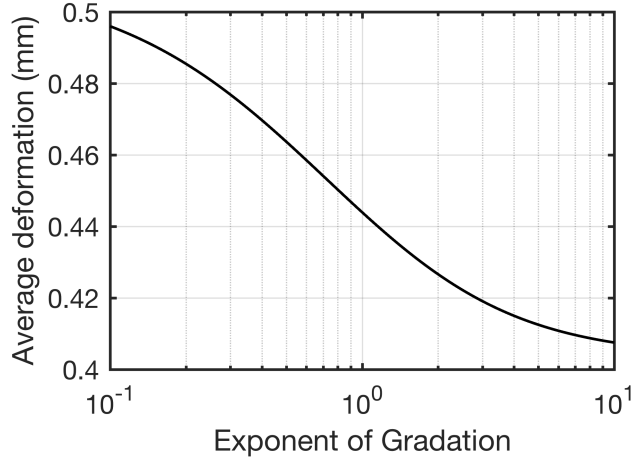


Figure 24: Average deformation against exponent of gradation for a disk of radius of 100 mm. Minimum occurs at right endpoint, where $m = 10$ and “graded” material is almost entirely titanium.

3) Varying Materials in Top and Bottom Layers

We also examine the effect of using various materials as the top and bottom layer of our simulated circuit board, requiring that the bottom layer be a metal (excluding titanium due to cost), and that the top layer be a ceramic. In particular, the bottom layer can be stainless steel (SS316), aluminum (Al), alloy 42, kovar, or the nickel alloy Ni200. The top layer can be alumina ($rmAl_2O_3$), silicon carbide (SiC), or silicon nitride (SiNi). As before, we examine the temperature-averaged stress (in the ceramic layer) and deformation (with plate radius of 100 mm).

	Alumina	Silicon Carbide	Silicon Nitride
Stainless Steel	23.41	62.91	93.97
Aluminum	91.22	59.71	59.96
Alloy 42	48.08	81.47	106.44
Kovar	34.65	71.62	102.51
Nickel Ni-200	24.25	66.99	98.42

Figure 25: Temperature-averaged max stress in insulating layer for different materials, measures in megapascals (MPa). Temperatures range from 300K to 450K.

	Alumina	Silicon Carbide	Silicon Nitride
Stainless Steel	0.46	0.55	0.61
Aluminum	0.88	0.98	1.06
Alloy 42	0.16	0.07	0.01
Kovar	0.05	0.04	0.10
Nickel Ni-200	0.37	0.45	0.51

Figure 26: Temperature-averaged deformation for different materials, measures in millimeters (mm). Temperatures range from 300K to 450K. Disk radius is 100 mm.

These results in table 25 and 26 show that your quantity of interest is very important in reading the results. For example, if you are interested in the lowest deformation you would pick Alloy 42 and Silicon Nitride. However, if you are interested in the lowest max stress in the insulating layer you would choose Alumina and Nickel. Based on these results if you were trying to minimize both stress and deformation the best choice would be Alumina and Kovar.

3.3.2 Optimizing the thermal strain

After investigating the optimization of Problem A we began investigating how to optimize thermal strain. For the remainder of the subsection we investigate conditions that lead to the equality

$$\varepsilon_T = \varepsilon_B. \quad (37)$$

First let

$$AB_k \equiv A_k - B_k = \sum_{i=1}^N E'_i (z_i^k - z_{i-1}^k)$$

$$CD_j \equiv C_j - D_j = \sum_{i=1}^N \varepsilon_{th,i} E'_i (z_i^j - z_{i-1}^j),$$

so that

$$\varepsilon_T = \frac{1}{F} (CD_2(6hAB_1 - 3AB_2) + CD_1(4AB_3 - 6hAB_2))$$

$$\varepsilon_B = \frac{1}{F} (4AB_3CD_1 - 3AB_2CD_2),$$

with $F = 4AB_3AB_1 - 3(AB_2)^2$. Now we obtain for the condition (37) that

$$\varepsilon_T - \varepsilon_B = \frac{6h}{F} (CD_2AB_1 - CD_1AB_2) = 0.$$

That is, we are solving the condition

$$\frac{CD_2}{CD_1} = \frac{AB_2}{AB_1}.$$

In the remainder the unknowns are $E'_i, \varepsilon_{th,i}$ and the thicknesses $z_i - z_{i-1} = h_i$. Observe that $CD_2 = \sum_{i=1}^N \varepsilon_{th,i} E'_i h_i (z_i + z_{i-1})$ and that $AB_2 = \sum_{i=1}^N E'_i h_i (z_i + z_{i-1})$ so that

$$\frac{\sum_{i=1}^N \varepsilon_{th,i} E'_i h_i (z_i + z_{i-1})}{\sum_{i=1}^N \varepsilon_{th,i} E'_i h_i} = \frac{\sum_{i=1}^N E'_i h_i (z_i + z_{i-1})}{\sum_{i=1}^N E'_i h_i} = 0. \quad (38)$$

From 38 we may conclude that equality will hold whenever

$$\varepsilon_{th,i} = c, \quad \text{for all } i.$$

That is the thermal strain coefficient is the same for all materials included. Therefore we conclude that if the goal is to design a material that is robust under temperature changes, then it is advisable to select materials that have similar thermal strain properties. To verify this analytical result we construct a hypothetical structure that is equal to the structure from problem a), with the exception that we let the thermal strains in the middle layer be the same $\varepsilon_2^{th} = \varepsilon_3^{th} = \varepsilon_4^{th} = c$ and the ones in the remaining layers satisfy $\varepsilon_1^{th} = \varepsilon_5^{th} = F \cdot c$. Here $0 \leq F \leq 1$ is a fraction that measures how close the thermal strains are to each other. We find that the minimum for $|\varepsilon_T - \varepsilon_B|$ is precisely found when $F = 1$ or when all the strains are equal to each other:

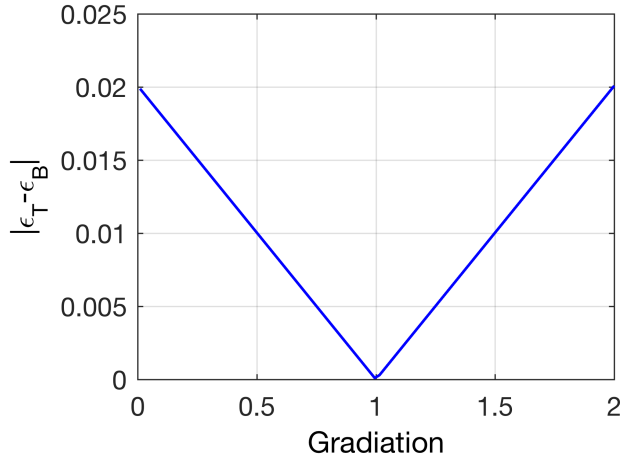


Figure 27: We vary the scalar F which measures how close the thermal strains for a 5 layered material are. At the point when $F = 1$ all materials have equal ε_i^{th} and $|\varepsilon_T - \varepsilon_B|$ is minimized.

3.3.3 Optimizaiton of Problem C

Our objective is to minimize the total structure deflection. Let the deflection be denoted by $\delta(h_1, h_2, N; T) = \delta(\mathbf{h}; N, T)$ in which $\mathbf{h} = [h_1, h_2]^T$, N vary and h is fixed for all temperatures. In particular we discretize the temperature as

$$T_j = T_0 + j \frac{T_1 - T_0}{J} = T_0 + j \Delta T, \quad 0 \leq j \leq J;$$

where T_1, T_0 denote the final and initial temperatures (Kelvin), respectively. Mathematically our optimization problem is

$$\underset{\mathbf{h} \in \mathbb{R}^2, N \in \mathbb{Z}^+}{\text{minimize}} \quad q(\mathbf{h}, N; T), \quad \text{subject to: } N(\mathbf{h}^T \mathbf{1}) = h,$$

where the objective function, q , is defined as

$$q(\mathbf{h}, N; T) = \frac{\Delta T}{T_1 - T_0} \sum_{j=1}^M |\delta(\mathbf{h}, N; T_j)|,$$

$0 < h$, and J is a fixed integer. This formulation of the problem requires optimization over continuous (\mathbf{h}) and an integer variable (N). Because the computation of the objective function is cheap, and the solution of mixed variables optimization problems is in general very hard, we decide to break down the problem into separate optimization problems for a specified number of layers. That is, we setup a grid of layers

$$N_i = i, \quad \text{where } i \in \{1, 2, \dots\},$$

which allows us to fix the integer variable N so that we obtain an objective functions that only depend on the continuous variable \mathbf{h} . We thus optimize M separate problems, for which the i^{th} problem is of the form

$$\underset{\mathbf{h} \in \mathbb{R}^2}{\text{minimize}} \quad q(\mathbf{h}; T, N_i), \quad \text{subject to: } N_i(\mathbf{h}^T \mathbf{1}) = h,$$

for $i = 1, 2, \dots$. In a particular scenario we set $h = 300\text{mm}$ and the materials as

$$\text{Material}_1 \equiv Al_2O_3, \quad \text{Material}_2 \equiv Al.$$

Moreover we set

$$\begin{aligned} T_0 \text{ (Lower temperature)} &= 298K, \\ T_1 \text{ (Upper temperature)} &= 800K, \\ T_{\text{ref}} \text{ (Reference temperature)} &= 600K, \\ J \text{ (# Temperature intervals)} &= 100, \\ h \text{ (Structure height)} &= 300\text{mm}, L \text{ (Half-length of structure)} &= 300\text{mm}, \end{aligned}$$

Our initial guess for the thicknesses (mm) is scaled by the number of pairs

$$\mathbf{h}_i = \frac{1}{i} [100 \quad 200]^T.$$

Our implementation uses the MATLAB function `fmincon` with an interior point algorithm that allows us to implement the nonlinear constraint.

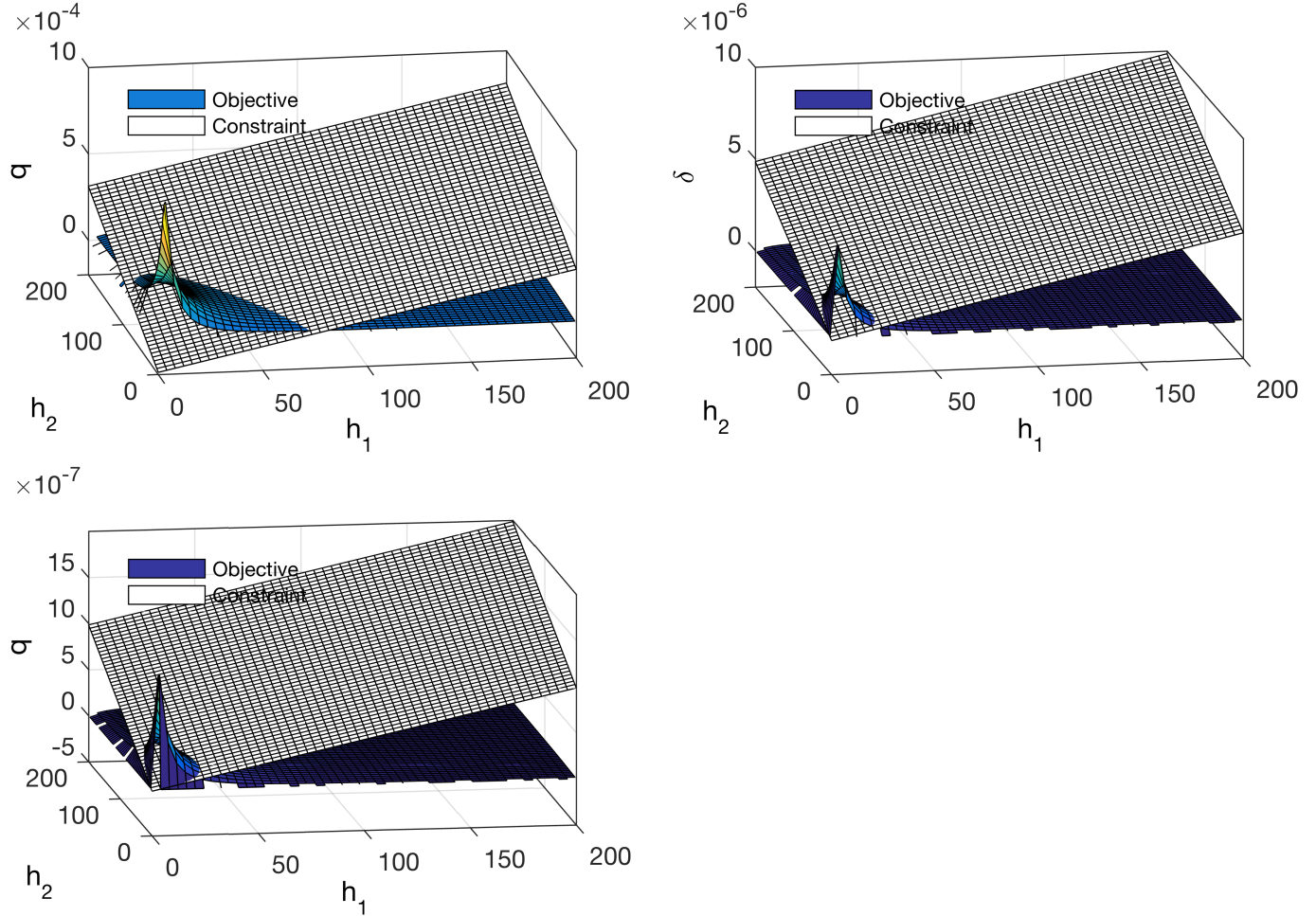


Figure 28: Plot of the objective function with a representation of the constraint for a different number of layers. As the number of layers increases the magnitude of the objective function decreases, although the general form of the objective does not change significantly.

For this problem we observe that the deflection of the material decreases as the number of pairs is increased. In particular we find that one setup may be slightly superior to the other ones. As a guide for designing a particular structure we display the ratio of the thicknesses that correspond to a solution of the optimization problem $\frac{h_2^*}{h_1^*}$

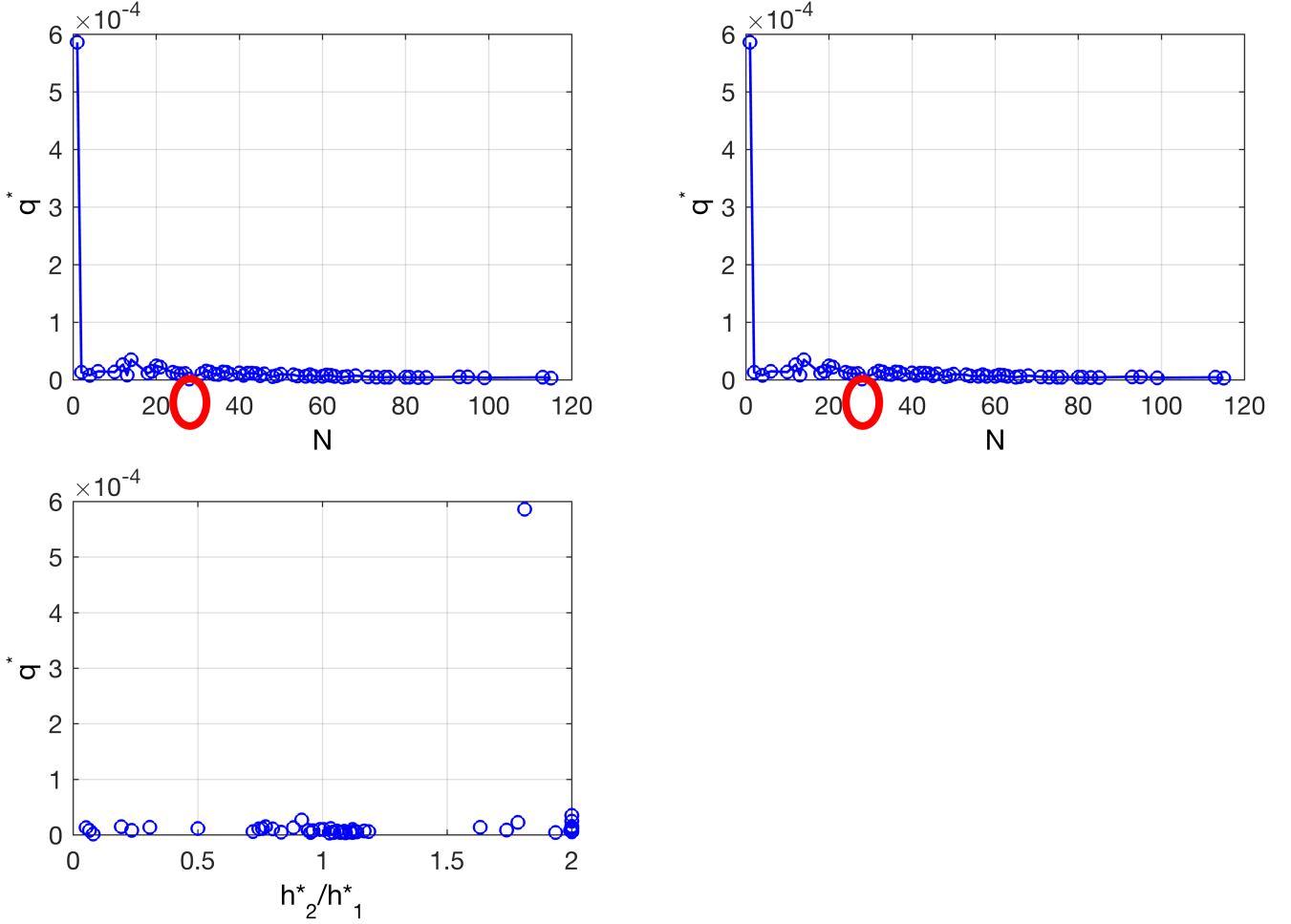


Figure 29: A plot of the objective function as the number of pairs in the structure is varied. It appears that a structure of $N = 28$ pairs has an objective value that is lower than its neighboring setups.

From Figure 28 and 29 it was seen that as the number of layers increases the magnitude of the objective function decreases, although the general form of the objective does not change significantly. It also appears that a structure of $N = 28$ pairs has an objective value that is lower than its neighboring setups. Solutions are found where the materials are equally thick or the second material is twice as thick as the first one.

3.4 Uncertainty

When analyzing a model, it is important to remember that any uncertainty in input parameters leads to uncertainty in the output. The uncertainty in the input is typically caused by random sources such as noise within measuring devices or subtle variation from one test specimen to another. Ideally, these influences are as controlled as much as possible to decrease the amount of uncertainty in the input. In the real world this can never be accomplished, but we can set reasonable bounds on the expected value for each input, often including some factor of safety. It then becomes important to observe and quantify how large of effect this input variation will have on the output.

To obtain the effect that input parameter uncertainty has on the output, one can employ Monte Carlo sampling. A statistically significant number of samples are taken of each input parameter and used to evaluate the model. The output will be different for each sampled set of parameter values. In some cases there are multiple quantities of interest in the output, and each one will have uncertainty. To visualize this uncertainty it is often a good idea to generate a histogram of the quantity of interest, which highlights the distribution of the output. One can also calculate typical statistical measures such as mean and standard deviation. An

example of the randomness of input variables is shown in Figure 30 on the left and a corresponding distribution of an output quantity of interest is shown in Figure 30 on the right.

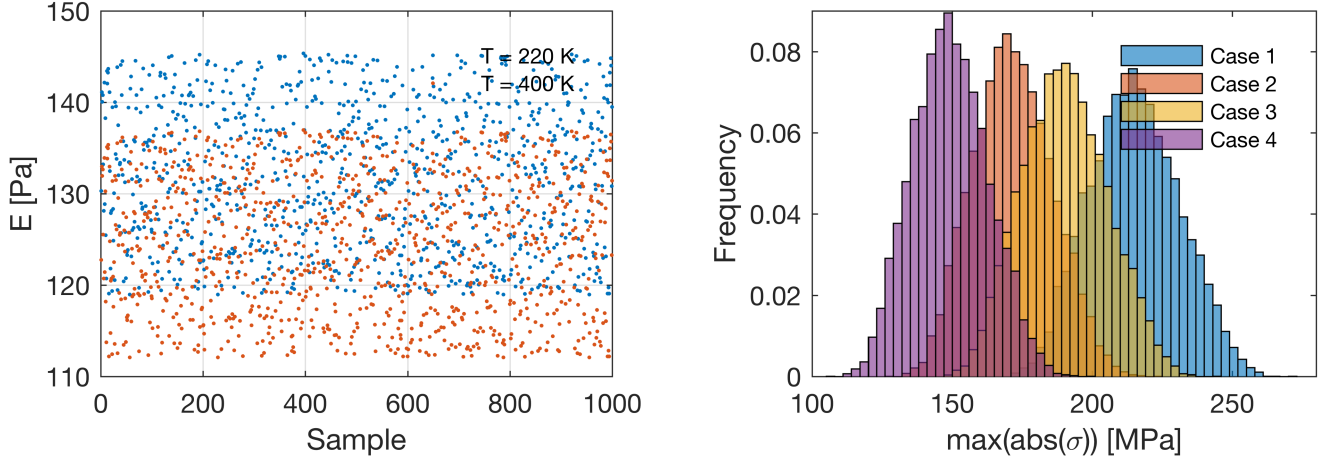


Figure 30: Uncertainty of input parameters (a) leads to uncertainty in output (b). Note the uncertainty from input to output is not necessarily a linear relationship.

One important observation to point out is that the distribution of output parameters will not necessarily match the distribution of the input parameters. In the cases reported below, we have assumed a uniform distribution about nominal parameter values. Upon evaluating the output based on a random sampling from these uniform distributions, the quantities of interest clearly do not have uniform distributions (see Figure 30). In other words the mapping from input to output is nonlinear.

The other observation to be made when considering uncertainty quantification is the deviation in the output. Refinement of input parameters may lead to reduced uncertainty in the output, but it may be at the expense of the design criteria. In other words, a given input may lead to a higher mean magnitude of stress, but with less deviation. This provides confidence that the results will be in the predicted range, which is often more important than simply reducing the magnitude of a certain quantity as much as possible.

The next question to be answered is how many samples to take? Pure random sampling is acceptable, but potentially cost prohibitive. An alternative approach is demonstrated in the Section 3.4.1.

3.4.1 Latin Hypercube Sampling

When employing Monte Carlo techniques, it is important to optimally sample the parameter space. Simply running pure random samples many times will lead to a converge density of the output as the number of samples go to infinity. How many samples are actually required is dependent on the problem, and potentially prohibited by cost. Alternatively, one can sample the input parameter space using the Latin Hypercube sampling method.

The basic premise of Latin Hypercube sampling is to optimally observe all combinations of defined input spaces. Picture a two-dimensional grid sampling space, where each cell corresponds to a sample position. If the points sampled from this space satisfy the requirement that no two points are in either the same row or column, then this is what is called a Latin square. Latin Hypercube is the multidimensional analogue to the square.

Given a set of P input variables that will be sampled N times, the corresponding number of combinations for a Latin Hypercube is

$$N^{P-1}. \quad (39)$$

The P input variables are divided into N equally likely intervals, and then N sample points are taken to satisfy the Latin Hypercube requirement. To demonstrate the effectiveness of this sampling strategy we consider a comparison with the random sampling method to quantify a particular quantity of interest. As

seen in Table 5 the mean and variance of the deflection for Case Study B at the lowest temperature (220 K) converges to a stable distribution as the number of samples increases. However, by using Latin Hypercube sampling the stable distribution is reached with orders of magnitude less samples.

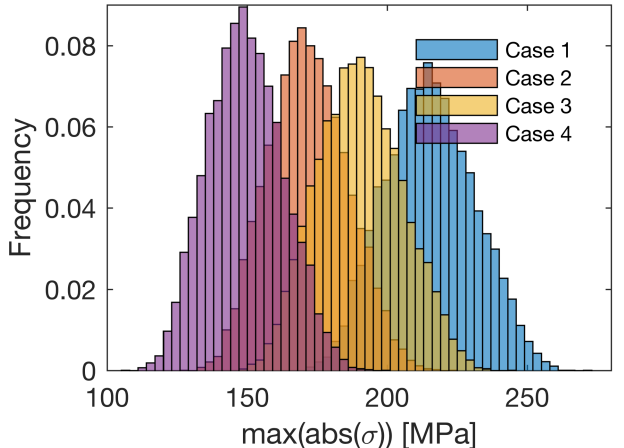
Random			Latin Hypercube		
$\log_{10}(N)$	μ	σ^2	$\log_{10}(N)$	μ	σ^2
2	-0.467	0.791	2	-0.463	0.786
3	-0.465	0.788	3	-0.463	0.786
4	-0.464	0.787	4	-	-
5	-0.464	0.786	5	-	-

Table 5: Mean and variance of deflection from Case Study B at $T = 220$ K. Using Latin Hypercube sampling converges to a stable output distribution much faster than a random technique. The mean values are reported in [mm] and the variance in [mm^2].

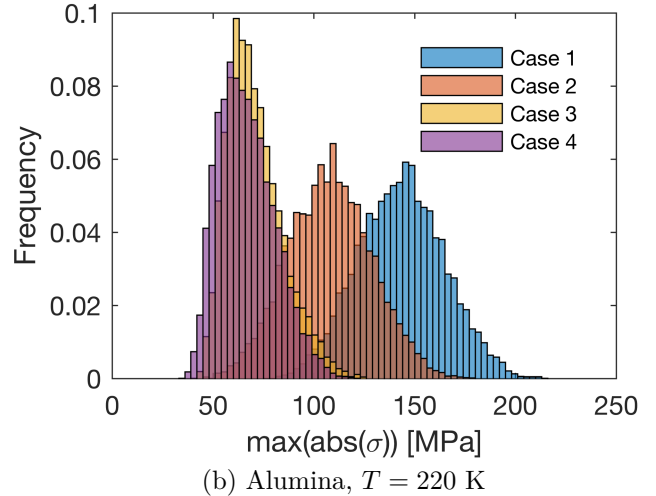
3.4.2 Uncertainty Problem A

For Problem A, we consider the effect of uncertainty in multiple input parameters. The material properties of Alumina, Stainless Steel, solder, and both ends of the graded layers are considered uncertain. In addition the thickness of each layer is assumed to have uncertainty and even the exponent of gradation. This leads to an input parameter space with 23 random variables. Each of these random inputs were assumed to have uniform variation, but as seen in Figure 31 the output uncertainty is not necessarily uniformly distributed.

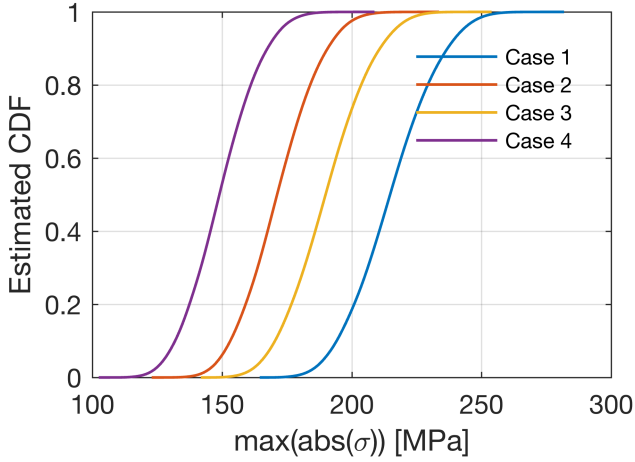
We can make several observations from the results seen in Figure 31. The lowest maximum magnitude of stress that occurs in the stainless steel layer occurs in Cases 2 and 4 when the solders on either side of the graded layer are thicker. Also, by changing the exponent of gradation to $m = 2$ in Case 4 there is an additional decrease in the maximum magnitude of stress. Because the graded layer goes from titanium to Invar, a exponent of 2 implies that the layer maintains properties more like titanium over the thickness. The lowest maximum magnitude of stress that occurs in the Alumina also appears to be for case 4; however, Case 2 does not decrease the stress as much as does Case 3. So, it appears that having properties more like Titanium through the graded layer decreases the stress for the Alumina, but the effect of solder thickness is not as clear. Depending on the desired use of the structure, one must also take into account the deflection or amount of deformation of the material. In Figure 32 it is seen that the deflection is smallest for Cases 2 and 4. This is in agreement with the analysis of the forward model.



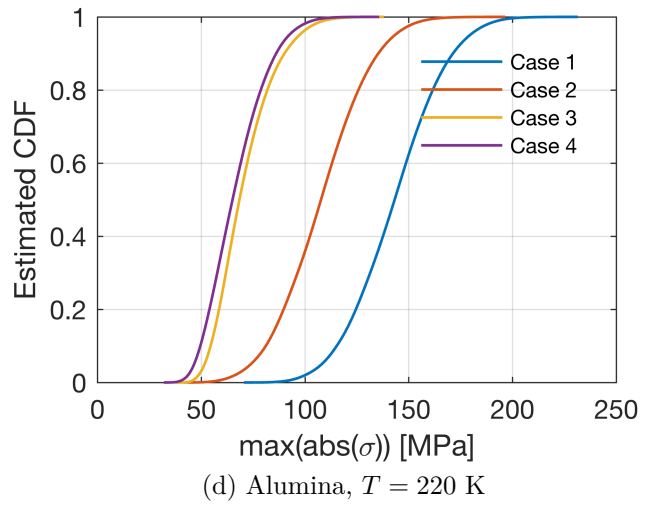
(a) Stainless Steel, $T = 220$ K



(b) Alumina, $T = 220$ K

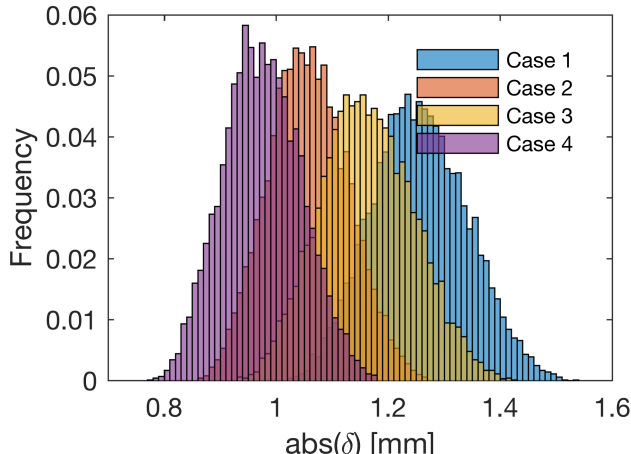


(c) Stainless Steel, $T = 220$ K

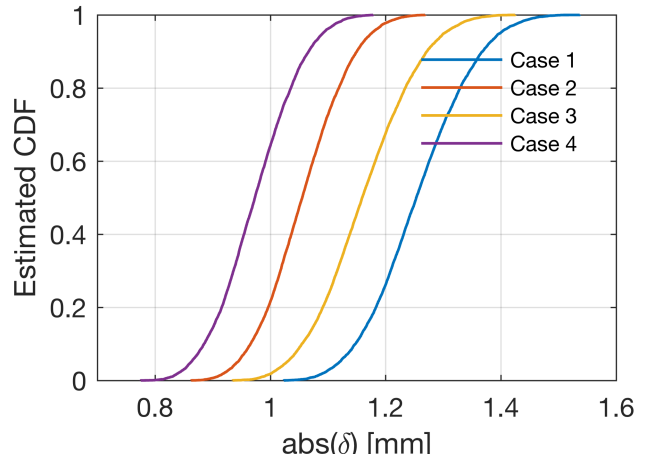


(d) Alumina, $T = 220$ K

Figure 31: Problem A - $T_{ref} = 456$ K: Maximum absolute stress in the layer of (a,c) Stainless Steel - SS316 and (b,d) Alumina - Al_2SO_3 . The first row of Figures represent normalized histograms. The second row are estimated cumulative distributions of the same quantity.



(a) Deflection, $T = 220$ K

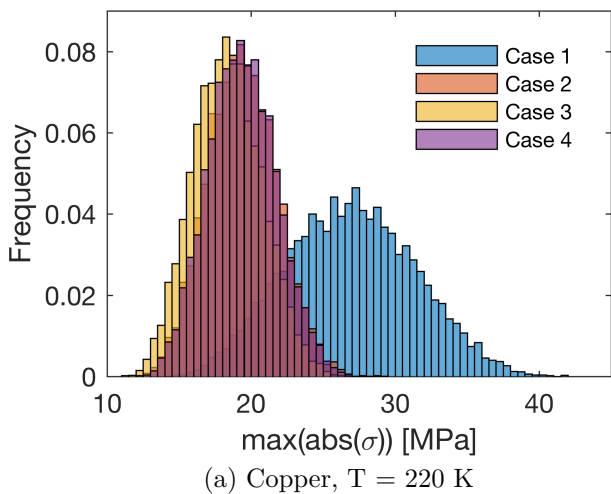


(b) Deflection, $T = 220$ K

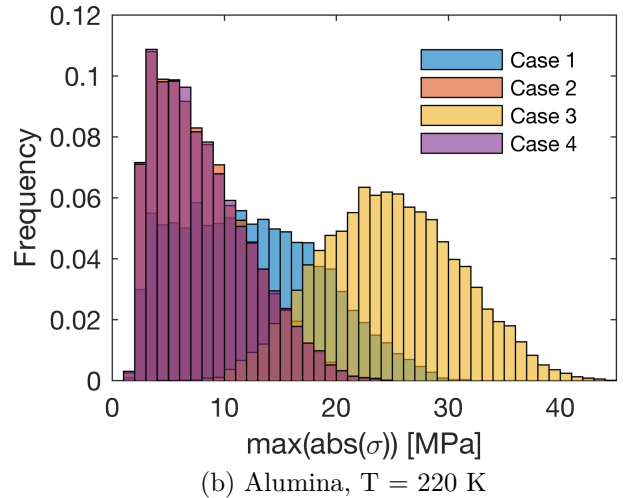
Figure 32: Problem A - $T_{ref} = 456$ K: Deflection of structure (a) Normalized Histogram and (b) Estimated CDF.

3.4.3 Uncertainty Problem B

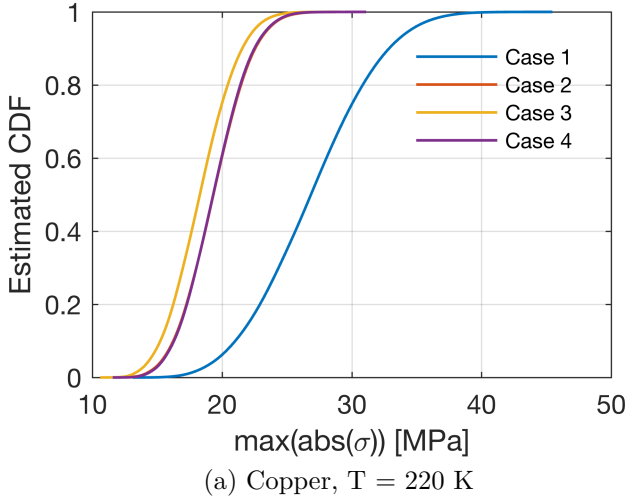
For Problem B we will also look at the maximum absolute value of stress in the bottom and top layer as well as the deflection.



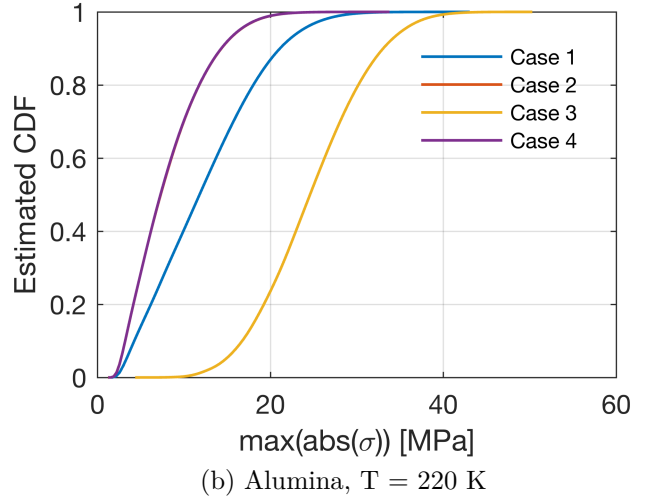
(a) Copper, $T = 220$ K



(b) Alumina, $T = 220$ K

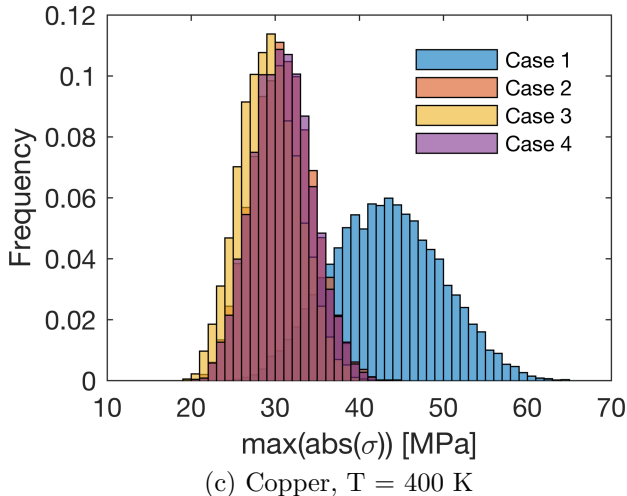


(a) Copper, $T = 220$ K

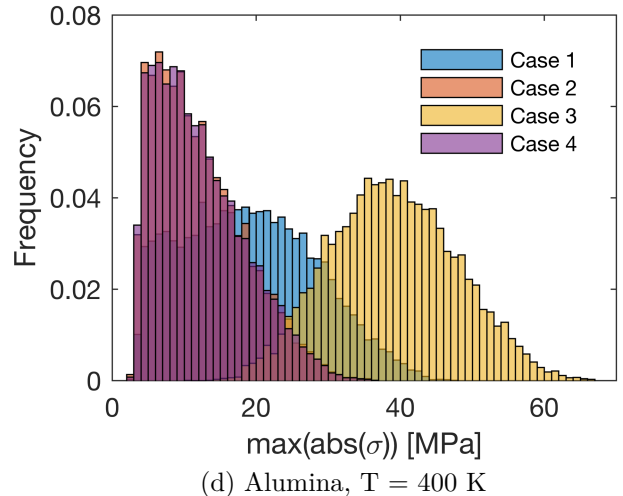


(b) Alumina, $T = 220$ K

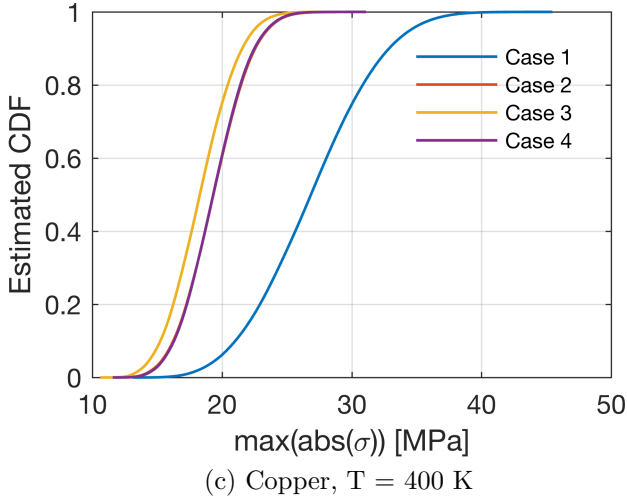
Figure 33: Problem B - $T_{ref} = 295$ K: Maximum absolute stress in the layer of (a,c) Copper - Cu and (b,d) Aluminum - Al. The histograms are normalized.



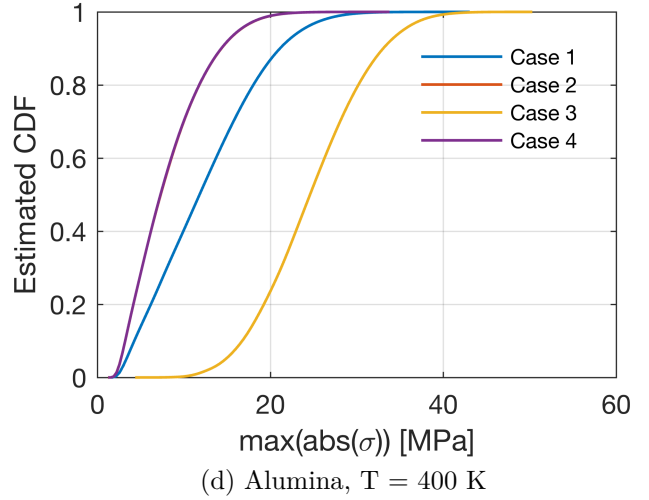
(c) Copper, $T = 400$ K



(d) Alumina, $T = 400$ K



(c) Copper, $T = 400$ K



(d) Alumina, $T = 400$ K

Figure 34: Problem B - $T_{ref} = 295$ K: Maximum absolute stress in the layer of (a,c) Copper - Cu and (b,d) Aluminum - Al. The histograms are normalized frequency.

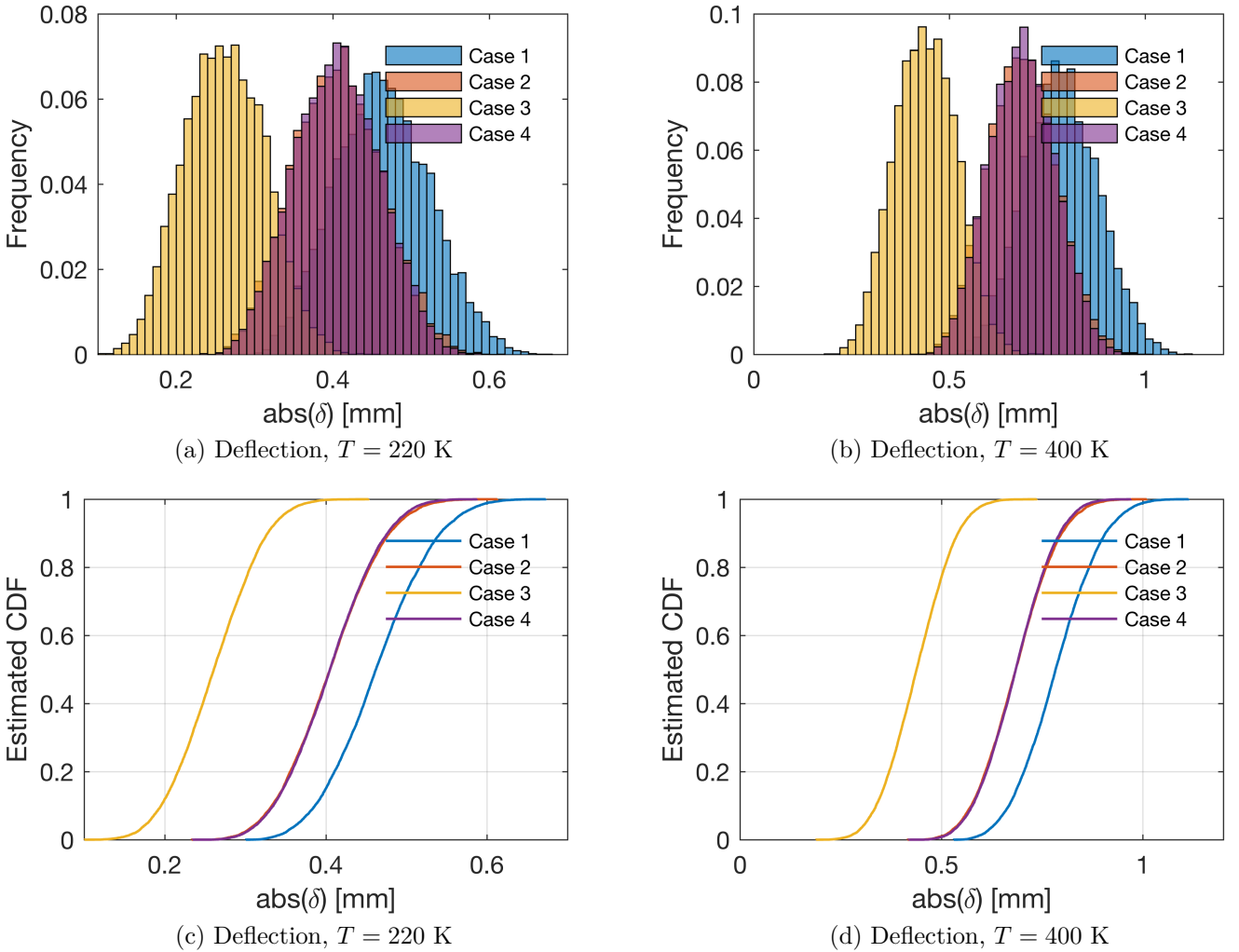


Figure 35: Problem B - $T_{ref} = 295$ K: Deflection of structure (a,b) Normalized Histogram and (c,d) Estimated CDF. (a,c). Note absolute value of deflection is report to ease the interpretation of the cumulative distribution plots.

As seen in Figures 33-35 the maximum magnitude of stress is very different depending on the operating temperature. Case 3 and 4 appear to reduce stress the most at the lowest temperature; however, at the highest operating temperature Case 3 results in a larger magnitude of stress in both the bottom and top layer. Depending on the criteria it may be important to have a design that produces similar results over the entire operating regime. Under those conditions Case 4 would be advantageous for reducing the stress because it works over a broader temperature range.

As opposed to problem A, the deflection is not necessarily minimized in the same way as the stress. The deflection is smallest for Case 3 at both the low and high temperatures as seen in Figure 35. If reducing the deflection in the structure is more important than reducing the stress, than Case 3 may be the best design choice. This highlights the complexity noted previously that the design choice is affected by many factors.

4 Summary and Recommendations

In conclusion, we developed a computationally efficient model for predicting the residual stress and deflection of multilayered structures. We started with the question of how to optimize the deflection and stress. From there we began to build on Hall's model and included the ability to deal with gradient layers and temperature

dependence. We then tested the model on three representative multilayered structures. Based on these problems we then looked at the sensitivity, optimization, and uncertainty quantification of the input variables and processing parameters.

Based on the testing we saw that the optimal design depends much on what are the application and design criteria. Optimizing one criterion may be detrimental to another. The way a particular structure should be made leads to different strategies and therefore different optimizations. Sensitivity analysis highlights that the change in quantities of interests with respect to the change of different parameters has a nonlinear trend. Also certain parameters have more impact on particular quantity than others. Therefore depending on the application and cost, the quantity of interests determine which parameters can be studied to achieve optimal output. From uncertainty analysis we observed how changes to the nominal design can result in improved reliability probabilistically. Finally we estimated that material gradation can significantly improve multilayered structure performance. Therefore, we suggest continued development of advanced manufacturing techniques.

5 Appendix

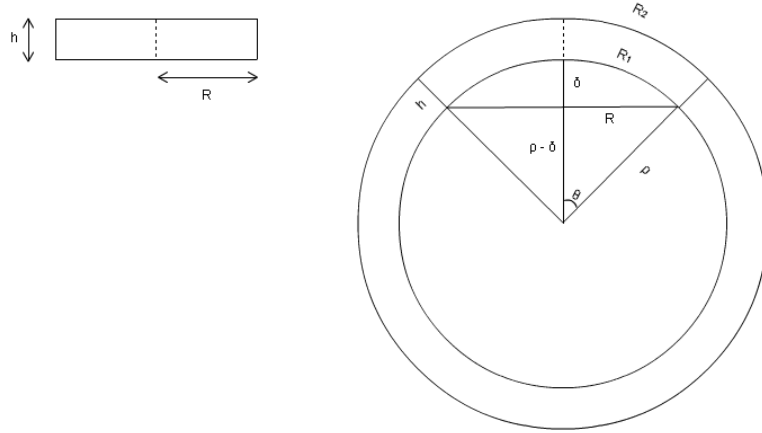


Figure 36: Diagram of the multilayer structure. On the left is the structure before thermal deformation. On the right is the structure after thermal deformation, with the circle completing the curve drawn in.

Figure 36 shows a multilayer structure of disk radius R and thickness h . The diagram on the left is the structure before thermal deformation. The diagram on the right is the structure after thermal deformation, with the circle completing the curve drawn in. We assume that the deformation is so small that the horizontal line segment from the end of the structure to the center remains R . The radius of curvature, deflection, angle of curvature, arc length of the bottom of the structure, and arc length of the top of the structure are ρ , δ , θ , R_1 , and R_2 , respectively. The bottom and top strains are given by

$$\varepsilon_B := \frac{\Delta R_1}{R} = \frac{\rho\theta - R}{R} \quad (40)$$

$$\varepsilon_T := \frac{\Delta R_2}{R} = \frac{(\rho + h)\theta - R}{R}, \quad (41)$$

where the arc length formula is used for the second equality. Subtracting the bottom strain from the top strain and rearranging yields

$$\theta = \frac{R}{h}(\varepsilon_T - \varepsilon_B). \quad (42)$$

Since

$$\sin \theta = \frac{R}{\rho}, \quad (43)$$

we have

$$\frac{R}{\rho} = \sin \left(\frac{R}{h} (\varepsilon_T - \varepsilon_B) \right), \quad (44)$$

from which we get the radius of curvature in terms of known quantities,

$$\rho = \frac{R}{\sin \left(\frac{R}{h} (\varepsilon_T - \varepsilon_B) \right)}. \quad (45)$$

Since the deformation, and thus the deflection, are so small, we can assume that the angle of deflection is also very small. This allows the approximation

$$\sin \theta \approx \theta. \quad (46)$$

Using this approximation in (42) and (43) and rearranging yields a simpler, but accurate, formula for the radius of curvature in terms of known quantities,

$$\rho = \frac{h}{\varepsilon_T - \varepsilon_B}. \quad (47)$$

From Figure 36, we obtain

$$(\rho - \delta)^2 + R^2 = \rho^2, \quad (48)$$

from which we get the deflection in terms of known quantities,

$$\delta = \rho - \sqrt{\rho^2 - R^2}. \quad (49)$$

References

- [1] B.E. Carroll et al. “Functionally graded material of 304L stainless steel and inconel 625 fabricated by directed energy deposition: Characterization and thermodynamic modeling”. In: *Acta Materialia* 108 (2016), pp. 46–54. ISSN: 13596454. doi: 10.1016/j.actamat.2016.02.019.
- [2] Peter M Hall. “Thermal expansivity and thermal stress in multilayered structures”. In: *Thermal stress and strain in microelectronics packaging*. Springer, 1993, pp. 78–94.
- [3] Claude A Klein and Richard P Miller. “Strains and stresses in multilayered elastic structures: The case of chemically vapor-deposited ZnS/ZnSe laminates”. In: *Journal of Applied Physics* 87.5 (2000), pp. 2265–2272. ISSN: 0021-8979.
- [4] Kenneth A Peterson and Robert D Watson. *Bi-level microelectronic device package with an integral window*. Jan. 2004.
- [5] X C Zhang et al. “Modeling of thermal residual stresses in multilayer coatings with graded properties and compositions”. In: *Thin Solid Films* 497.1 (2006), pp. 223–231. ISSN: 0040-6090.